Review

Metal–organic frameworks for heavy metal removal from water

Paulina A. Kobielska [a], Ashlee J. Howarth [b], Omar K. Farha [b], Sanjit Nayak [a,*]

[a] School of Chemistry and Biosciences, Faculty of Life Sciences, University of Bradford, Richmond Road, Bradford, West Yorkshire BD7 1DP, United Kingdom
[b] Department of Chemistry, Northwestern University, 2145 Sheridan Road, Evanston, IL 60208, United States

ARTICLE INFO	ABSTRACT
	The pollution of surface and groundwater with heavy metals is a serious global concern, both environmentally, as well as with respect to human health. Overabundance of these elements poses severe health risks for humans, and also for other life forms through bioaccumulation along food chains. Therefore, steps should be taken to reduce the amount of such elements in water to acceptable levels. This review looks at metal–organic frameworks (MOFs) which have been recently developed and studied for potential applications in heavy metal removal from water. We provide an overview of the current capabilities and important properties of MOFs used for this purpose. © 2017 Elsevier B.V. All rights reserved.

Contents

1. Introduction

1.1. Sources of heavy metals in water

Geological sources: Heavy metals (that is metals with density over 5 g cm^{-3} such as arsenic, cadmium, chromium, copper, lead, mercury, nickel and zinc) [1] polluting our water is a rapidly growing global concern. These elements can be found within the environment – be it in water reservoirs, the atmosphere or soil – in excess, due to various anthropogenic actions. It is also important to note the natural sources of heavy metal pollution. These include all types of rocks (igneous, sedimentary and metamorphic), which, through their interactions with the surrounding environment (i.e., weathering, erosion, soil formation and the rock cycle in general), transport and redistribute heavy metals [2]. Heavy metals most commonly found in rock-forming minerals include those which most easily leach due to mineral weathering such as nickel, cobalt, manganese, zinc, copper, and vanadium, in addition to metals that have intermediate stability such as scandium, yttrium and other

* Corresponding author.
   E-mail address: s.nayak@bradford.ac.uk (S. Nayak).

Table 1
Anthropogenic sources for common heavy metal pollutants [3] along with their provisional guideline limits according to WHO [9] and their toxicity [7].

Heavy metal	Anthropogenic sources	Provisional maximum tolerable daily intake (PMTDI) (g L^{-1})	Toxicity
As	Animal feed additive, algaecides, herbicides, insecticides, fungicides, pesticides, rodenticides, sheep dip, tanning and textile, pigments, veterinary medicine, ceramics, special glasses, metallurgy, electronic components, non-ferrous smelters, electrical generation (coal and geothermal), light filters, fireworks	0.01	Phytotoxic (toxic to plants), arsenicosis (i.e., blackfoot disease), keratosis, possible vascular complications, carcinogenic
Cd	Neutron absorbers (within nuclear reactors), nickel–cadmium batteries, anti-corrosive metal coatings, alloys, plastic stabilizers, coal combustion, pigments	0.003	Phytotoxic, bio-accumulative, *itai-itai* disease, carcinogenic
Cr	Data storage, plating, ferro-alloys manufacturing, textiles and leather tanning, wood treatment, passivation of corrosion of cooling circuits, pigments	0.05	Cr^{3+} not detrimental to mammals, Cr^{6+} very toxic, carcinogenic
Cu	Water pipes, chemicals and pharmaceutical equipment, kitchenware, roofing, alloys, pigments	2	Relatively not detrimental, narrow tolerance for plants
Pb	Alloys, ceramics, plastics, glassware, lead-acid batteries, cable sheathings, sheets, solder, pipes and tubing, sheets, ordinance, antiknock agents, tetramethyllead, pigments	0.01	Pb poisoning (a world-wide issue) through gasoline, plumbing and paints
Hg	Amalgamation (the process of metal extraction), electrical and measuring apparatus, catalysts, dental fillings, Hg vapor lamps, solders, X-ray tubes, pharmaceuticals, fungicides, scientific instruments, electrodes, rectifiers, oscillators, chloralkali cell's mobile cathode.	0.006	Biomagnification in aquatic environments, Minamata disease
Ni	An alloy in the steel industry, computer components, catalysts, ceramic and glass molds, electroplating, nickel–cadmium batteries, dental and surgical prostheses, arc-welding, rods, pigments	0.07	Contact dermatitis, asthma, chronic respiratory infections carcinogenic
Zn	Zn alloys, PVC stabilizers, gold precipitation from cyanide solution, in chemicals and medicines, anti-corrosion coating, cans, barriers, rubber industry, welding and soldering fluxes, paints	0.3–1.0 mg kg^{-1} of body weight per day	Relatively not detrimental to mammals (may affect cholesterol metabolism in humans)

rare earth elements, all the way to uranium or hafnium, which can be found in zircon and are resistant to weathering. These elements are then concentrated when hot hydrothermal fluids permeate the rocks, inducing chemical reactions that cause precipitation of minerals and creation of ores [3]. Such deposits are often found within sedimentary rocks, which, due to their porous structure and high permeability, are well suited for storage of solids.

Soils are another medium responsible for heavy metal storage. Heavy metals in soil are found in relocated rock debris, insoluble minerals and organic matter (i.e., the solid phases), as well as in the water and air trapped within the soil (i.e., the fluid phases). These solid and fluid phases interact with each other and various ions passing through the system [4]. The concentration and identity of heavy metals in soil is directly related to the type of rock that the soil originated from. Most heavy metals can be found within the third layer – or horizon – of soil called the B-horizon. This layer contains elements which were once dissolved within the upper layer (the A-horizon) and then underwent eluviation (movement of the dissolved material downwards or sideways) into the lower layer, where they were deposited [5]. The B-horizon attracts heavy metals because it has a high concentration of iron oxyhydroxides and clay which are able to absorb the cationic elements [3].

Surface waters (from springs and streams to lakes and rivers) can carry heavy metals over a large distance and their chemical composition varies depending on the geological features over/ around which they flow. Other factors contributing to the identity and concentration of heavy metals in surface water include biological, chemical and physical influences such as living organisms, adsorption from sediments or organic and inorganic matter, dilution and evaporation, redox potential, pH and finally temperature [3]. For instance, increasing acidity (as the water flows over pyrite, which causes minerals to oxidize) influences the solubility of heavy metals and so increases their mobility within the water

[6]. Heavy metals carried by water can be adsorbed by oxyhydroxides or onto aquatic vegetation such as algae, introducing them into the food web. This leads to bioaccumulation of heavy metals within living organisms, causing toxicity and damage [2]. It is important to note that even though many heavy metals are essential to biological systems (e.g., copper, zinc), their intake over the provisional maximum tolerable daily intake can cause toxicity (see Table 1).

Anthropogenic sources: Groundwater reservoirs which are the main source of drinking water and of great importance to humankind, are contaminated mainly by organic and inorganic pollutants of anthropogenic origin. This pollution may lead to the poisoning of both aquatic and land animals, and ultimately poses a risk to human health. Monitoring and controlling potential sources of pollution is therefore vital. This includes sources such as runoff from agricultural and industrial sites, urban areas, mining and hazardous disposal sites, landfills, dredged sediments, sewage systems, railways and motorways [3]. Groundwater contamination can also result in redistribution of heavy metals throughout the environment, be it *via* uptake by plants or sorption/complexation (to particulate organic matter). A general overview showing the transportation of heavy metals within groundwater systems is illustrated in Fig. 1. Many human activities that contribute to heavy metal pollution can be tied, in broad terms, to the processes of production, consumption and disposal of products, across areas ranging from industry to agriculture and transportation. A summary of selected heavy metals and some of their anthropogenic sources are summarized in Table 1. The elements released by such activities can come both from diffuse, as well as point sources and are introduced into the environment as either gasses or particulates in aqueous or solid forms. Agricultural sources of pollution include substances used for crop management such as fertilizers. Phosphatic fertilizers for example contain cadmium and zinc in proportions dependent upon the type of rock they are derived
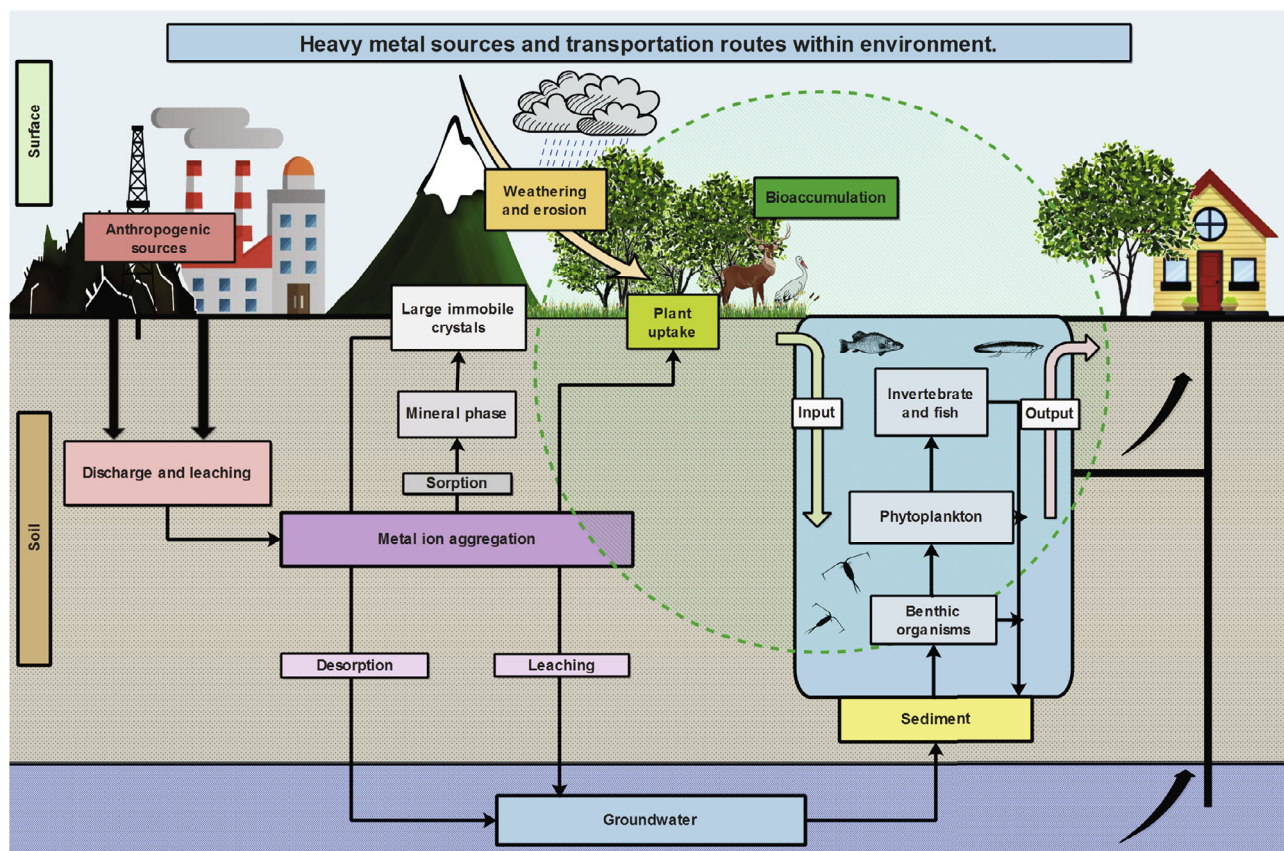
Fig. 1. A flowchart showing how soil, fresh- and groundwater systems redistribute heavy metals of anthropogenic origin [7]. *(Prepared using Edraw Max 7.9.)*

from: higher Cd content for sedimentary derivatives and lower for igneous rock derivatives [7]. Pesticides no longer contain heavy metals, however past usage of metal-rich products led to accumulation of arsenic, lead and mercury within soil and groundwater. Sewage effluents have been commonly used for soil enrichment during the past 100 years due to their high nutrient content. Despite their advantages, sewage effluents can also contain boron, cadmium, copper, lead, nickel and zinc which may cause toxicity in plants [3].

Industrial activities are also major contributors to heavy metal pollution in the environment. This is of particular concern for areas of the world that have yet to introduce modern legislation regarding this matter. The main industrial sources of pollution include mining, coal combustion, wastewater and the disposal of product waste. Mining produces large quantities of waste rock, still containing trace heavy metals (As, Cu, Cd, Pb, Hg), which are deposited within mine tailings and exposed to weathering and oxidizing conditions leading to acid drainage. This in turn mobilizes the heavy metals, which then permeate into the surrounding rock, soils and in some cases drinking water sources. Another industrial source of pollution, fossil fuel combustion, contributes mainly toward atmospheric heavy metal (As, Cd, Mo, Zn and Pb from gasoline additives) pollution. Solid waste from industrial processes is another major contributor to pollution due to the common lack of oversight over disposal sites allowing the waste to come in contact with soil or groundwater.

1.2. Materials in use for heavy metal separation from water

As discussed in the previous sections, heavy metals may originate from many different sources leading to accumulation in the environment and steps must be taken to reduce their release and

subsequent build-up. One way to mitigate the problem is to develop methods by which such elements can be removed from water. Within the last couple of decades a number of methods have been explored for heavy metal removal from water including ion exchange, membrane filtration, chemical precipitation, electrochemical treatment technologies and adsorption [8]. Due to its effectiveness, economic value, design/operation flexibility, and possible reversibility, adsorption techniques are currently among the most widely used remediation technologies [1].

One type of material that has been explored extensively for adsorptive heavy metal removal is metal oxides, including nanosized metal oxides (NMOs) which are characterized by their large surface areas and high activity. There are, however, issues with NMOs related to stability due to their nanoscale size, which leads to aggregation (caused by Van der Waals forces etc.) and subsequent decreases in efficiency. Impregnation onto porous supports (such as natural materials, synthetic polymeric hosts and activated carbon) has been shown to greatly improve the stability of NMOs [9]. Magnetic NMOs have also been studied and are of interest due to their magnetism which allows for easy separation from water when a magnetic field is applied [10].

Another class of adsorbent that is efficient, readily synthesized and commonly used, is zeolites. There are over 40 types of natural zeolites and more than 100 synthetic varieties. Naturally occurring zeolites, such as clinoptilolite (which is the most abundant type), are formed by crystallization of volcanic glass shards within volcanic ash rocks (i.e., tuff) and subsequent interaction with sea- or freshwater [11]. These are crystalline, cage and channel-like structures of aluminosilicate (tetrahedral AlO_4 and SiO_4). Zeolites have moderate surface areas, uniform pores and excellent ion exchange capabilities, which is due to the overall negative charge of the material. The negative charge results from Si^{4+} cations, which

occupy the central position within the tetrahedron, undergoing isomorphous substitution with Al^{3+} cations. Natural zeolites can be modified to increase their effectiveness for heavy metal removal from water. To this end, processes such as acid/base treatment or ion exchange causing surfactant impregnation are used. Synthetic zeolites are artificially synthesized from abundant (found, for instance, in clay) natural minerals: alumina and silica. These minerals can also be obtained from waste matter such as coal fly ash (CFA), which is a good source of amorphous, crystalline alumina-silicate, from which over 15 types of zeolites (including NaX, NaA, NaP1, NaY, Linde F or Kchabazite) can be synthesized. Other waste products such as ash (from rice husk, incineration, oil shale), municipal solid waste (examples include NaP1, NaX, ZSM-5 and ZSM-48) or cupola slag (ZSM-5, NaA and NaX) can also be used [12].

1.2.1. Metal–organic frameworks as adsorbents

Metal–organic frameworks (MOFs) are a class of adsorbent materials that have emerged within the past three decades. MOFs are constructed of secondary building units (SBUs) which are namely, metal ions or metal clusters, and organic linkers, which are connected into three-dimensional lattices. MOFs stem from polyhedral, or small cluster coordination polymers, which were later extended into one-dimensional chains, two-dimensional layers and finally three-dimensional frameworks. MOFs have numerous advantages when considering their use as adsorbent materials. One advantage is the high surface area and porosity of MOFs which is also advantageous for applications in gas storage, separation, catalysis, and drug delivery, among others [13]. High surface area and porosity can aid with adsorption site accessibility and diffusion of contaminants through the framework. Owing to their crystalline structure, MOF pores are highly ordered and the size of the pores as well as their shape, can be adjusted by choosing the linkers used as well as the connectivity of the metal ions [14]. MOFs can be designed to have ultra-high surface area and to date [15–19], a MOF reported by Farha et al. in 2012, has the largest BET area of any porous material at $\sim$7000 $m^2\,g^{-1}$ while computer simulations have shown that the upper limit of BET surface area for MOFs is $\sim$14,600 $m^2\,g^{-1}$, higher than previously expected [20]. Additionally, MOFs can be tuned *via* post-synthetic modification (PSM), to customize the ways in which they interact with guest molecules.

The use of MOFs in removing pollutants from water is a growing area of research and this report will focus on the recent developments in heavy metal removal [21–23]. Grouped by heavy metal, the effectiveness of MOFs that have been synthesized and tested to date will be discussed. Details of each framework and its properties, to give a broader picture of advantages and disadvantages of each material, are also included. The review will conclude with a summary and outlook for potential application of MOFs in removal of heavy metals from water.

2. Heavy metal uptake in MOFs

Metal–organic frameworks that have been studied for the removal of heavy metal ions from water are described. Table 2 summarizes all the studies that are discussed with an overview of the key information found within the literature reports. Table 2 is sorted according to metal ions, followed by the name of the MOFs used (or chemical formula), adsorption capacity, uptake mechanism, uptake time and optimal pH. What follows, is a set of subsections, divided by metal adsorbed and discussing the findings of each study in detail (based on information provided by the authors of each report).

2.1. Arsenic

Zhu et al. reported in 2012 the synthesis and arsenic (V) adsorption capabilities of **Fe-BTC** – a MOF containing iron nodes and 1,3,5-benzenetricarboxylic acid linkers. The MOF was synthesized using an autogenous pressure synthesis. During adsorption analysis, the pH (which controls the speciation of arsenic) was regulated using NaOH and HCl, and it was found that between pH 2 and 10 the removal efficiency of As(V) using Fe-BTC was greater than 96%, with the initial As(V) concentration being 5 mg/L and an optimum pH of 4. The material was found to be 37 times more effective than commercially available powdered iron oxide and 7 times more effective than Fe_2O_3 nanoparticles (50 nm size). Transmission electron microscopy (TEM) confirmed As(V) adsorption on interior sites of the MOF while IR measurements suggest interaction with the Fe nodes of the framework as supported by the appearance of a new IR band at 824 cm^{-1} corresponding with Fe–O–As groups [24]. In 2014, Jian et al. found that **ZIF-8** (zeolitic imidazolate framework-8) had moderate capacities for As(V) and As(III), of 49 $mg\,g^{-1}$ and 60 $mg\,g^{-1}$ respectively, achieved at neutral pH. The sources of the metal ions were $NaAsO_2$ and $Na_3AsO_4\cdot12H_2O$ for As(III) and As(V), respectively. The MOF itself was synthesized at room temperature using a slightly modified method. The adsorption rate of As species in ZIF-8 was found to be controlled by diffusion between particles rather than diffusion through the MOF pores – likely because the As species are too large to fit through the apertures of ZIF-8 meaning that uptake occurs on the surface sites of the framework [25]. In 2015, Liu et al. described three **ZIF** morphologies, namely cubic (**C**), leaf-shaped (**L-S**) and dodecahedral (**D**) as effective adsorbents for As(III). It was found that the adsorption capacity did not correlate with the MOF surface area, as the leaf-shaped ZIF (having a nearly ten-fold smaller surface area), had adsorption values only slightly lower than the other two morphologies. The dodecahedral ZIF was found to be the most stable framework, as confirmed by XRD and scanning electron microscopy (SEM) (Fig. 2) of the spent material. Fourier transform infrared spectroscopy (FT-IR) and X-ray photoelectron spectroscopy (XPS) analyses suggested the adsorption mechanism to be a surface hydroxyl substitution of Zn-OH on the surface of the MOF [26]. Vu et al. in 2015, gave details about the adsorption of As(V) in **MIL-53(Fe)** demonstrating an adsorption capacity of 21 $mg\,g^{-1}$. The MOF was synthesized *via* HF free-solvothermal methods. The adsorption mechanism was suggested to be based on a Lewis acid-base interaction between the anionic $H_2AsO_4^-$ species and the MOF node [27]. Li et al. described the use of a similar MOF in 2014 – **MIL-53(Al)**, which exhibited a maximum adsorption capacity of As(V) in the form of $HAsO_4^{2-}$ of 106 $mg\,g^{-1}$ at an optimum initial pH of 8. FT-IR and XPS data suggest the adsorption mechanism for As(V) in **MIL-53(Al)** is due to hydrogen bonding and electrostatic interactions. The structural integrity of the framework was preserved throughout the experiments and no aluminum ions were detected in the solution. The MOF was also found to be effective for As(V) removal in the presence of other anions, except for PO_4^{3-}, where its removal capacity dropped to 14% of the original value [28]. **MOF-808** was suggested by Li et al. in 2015 as another As(V) adsorbent. The MOF was synthesized in this report by irradiation with a household microwave. The crystals obtained by microwave synthesis were smaller (150–200 nm) than those obtained by typical solvothermal synthesis which helps to promote diffusion. The adsorption capacity of the MOF was found to be 25 $mg\,g^{-1}$ when the solution pH was adjusted to 4 using HCl. With an initial concentration of 5 ppm, rapid adsorption allowed for 95% of the As(V) molecules to be removed from solution within the first 30 min. The adsorption mechanism was suggested to be related to weak interactions between the As(V) ions and the Zr sites in MOF-808 [29]. In

Table 2

An overview of the key information on the MOFs discussed in this review. The Table is sorted according to metal ions, followed by the name of the MOFs used (or chemical formula), adsorption capacity, sources of metal ions, uptake mechanism, uptake time and optimal pH for adsorption. n/d is not disclosed.

Metal	MOF	Adsorption capacity (mg g^{-1}) of M ion	Metal ion source	Method	Time to adsorption equilibrium (min)	Optimal pH	Refs.
As	UiO-66	303 As(V)	Na$_2$HAsO$_4$·7H$_2$O	Adsorption	2880	2	[31]
	C; F–S; D ZIF	127; 108; 118 As(III)	NaAsO2	Adsorption	600	8.5	[27]
	MIL-53(Al)	106 As(V)	Na$_3$AsO$_4$·12H$_2$O	Adsorption	660	8	[29]
	ZIF-8	50 As(III); 60 As(V)	NaAsO$_2$; Na$_3$AsO$_4$·12H$_2$O	Adsorption	420 for As(V); 780 for As(III)	7	[26]
	MOF-808	25 As(V)	Na$_3$AsO$_4$	Adsorption	30	8	[30]
	MIL-53(Fe)	21 As(V)	n/d	Adsorption	90–120	6–7	[28]
	Fe-BTC	12 As(V)	Na$_3$AsO$_4$	Adsorption	10	4	[25]
Cd	Manganese MOF	176 Cd(II)	Cd(NO$_3$)$_2$·4H$_2$O	Adsorption	60	5	[52]
	Cu-terephthalate MOF	100 Cd(II)	Cd salt/Sungun wastewater	Adsorption/ion exchange	120	7	[40]
	HS-mSi@MOF-5	98 Cd(II)	n/d	Adsorption	30	6	[38]
	Cu$_3$(BTC)$_2$-SO$_3$H	89 Cd(II)	CdCl$_2$·2H$_2$O	Adsorption	10	6	[33]
	UiO-66-NHC(S)NHMe	49 Cd(II)	n/d	Adsorption	240	–	[36]
	TMU-5	43 Cd(II)	Cd(NO$_3$)$_2$·4H$_2$O	Adsorption	15	10	[39]
	AMOF-1	41 Cd(II)	n/d	ion exchange	1440	–	[34]
	HKUST-1-MW@H$_3$PW$_{12}$O$_{40}$	33 Cd(II)	n/d	Adsorption	80	7	[41]
	3D Co(II) MOF or (1)	70% Cd(II)	Cd(NO$_3$)$_2$·4H$_2$O	Adsorption	100	6	[37]
	PCN-100	1.6 Cd(II) per formula (ICP)	Cd(NO$_3$)$_2$	Adsorption	2880	–	[35]
Cr	MOR-1-HA	280 (±19) Cr(VI)	Cr$_2$O$_7^{2-}$ solution	ion exchange	60	3	[49]
	ZJU-101	245 Cr(VI)	Cr$_2$O$_7^{2-}$ solution	ion exchange	10	–	[46]
	TMU-30	145 Cr(VI)	K$_2$CrO$_4$	Adsorption	10	5.6	[48]
	TMU-5	123 Cr(III)	Cr(NO$_3$)$_3$·9H$_2$O	Adsorption	15	10	[39]
	UiO-66-NHC(S)NHMe	117 Cr(III)	n/d	Adsorption	240	–	[36]
	Chitosan-MOF	94 Cr(VI)	K$_2$Cr$_2$O$_7$	Adsorption	480	2	[43]
	Cu-BTC	48 Cr(VI)	K$_2$Cr$_2$O$_7$	Adsorption	–	7	[44]
	1-NO$_3$	37 Cr(VI)	K$_2$Cr$_2$O$_7$	ion exchange	240	5	[45]
	Fe$_3$O$_4$@MIL-100(Fe)	18 Cr (VI)	n/d	Adsorption	120	2	[42]
	ZIF-67	15 Cr(VI)	K$_2$Cr$_2$O$_7$	Adsorption/ion exchange	20–60	5	[47]
Pb	MnO$_2$-MOF	917 Pb(II)	Pb(NO$_3$)$_2$	Adsorption	60	5	[52]
	MOF-5	659 Pb(II)	n/d	Adsorption	30	5	[53]
	MIL-53(Al@100aBDC)	492 Pb(II)	Pb(NO$_3$)$_2$	Adsorption	360	–	[50]
	HS-mSi@MOF-5	312 Pb(II)	n/d	Adsorption	30	6	[38]
	TMU-5	251 Pb(II)	Pb(NO$_3$)$_2$	Adsorption	15	10	[39]
	UiO-66-NHC(S)NHMe	232 Pb(II)	n/d	Adsorption	240	–	[36]
	HKUST-1-MW@H$_3$PW$_{12}$O$_{40}$	98 Pb(II)	n/d	Adsorption	10	7	[41]
	Cu-terephthalate MOF	80 Pb(II)	Pb salt/Sungun wastewater	Adsorption/ion exchange	120	7	[40]
	AMOF-1	71 Pb(II)	n/d	ion exchange	1440	–	[34]
	Dy(BTC)(H$_2$O)(DMF)$_{1.1}$	5 Pb(II)	Pb(NO$_3$)$_2$	Adsorption	10	6.5	[51]
	3D Co(II) MOF or (1)	70% Pb(II)	Pb(NO$_3$)$_2$	Adsorption	100	6	[37]
Hg	BioMOF	900 HgCl$_2$; 166 CH$_3$HgCl	HgCl$_2$; CH$_3$HgCl	Adsorption	30 to 120	7	[65]
	UiO-66-NHC(S)NHMe	769 Hg(II)	n/d	Adsorption	240	–	[36]
	Thiol-HKUST-1	714 Hg(II)	HgCl$_2$	Adsorption	120	–	[54]
	[Ni(3-bpd)$_2$(NCS)$_2$]$_n$	713 Hg(II)	Hg(NO$_3$)$_2$	Adsorption	120	–	[58]
	FJI-H12	440 Hg(II)	HgCl$_2$	Adsorption	60	7	[55]
	LMOF-263	380 Hg(II)	HgCl$_2$	Adsorption	30	4–10	[61]
	Zn(hip)(L)·(DMF)(H$_2$O)	333 Hg(II)	Hg(NO$_3$)$_2$	Adsorption	60	5	[57]
	Fe$_3$O$_4$@SiO$_2$@HKUST-1	264 Hg(II)	HgCl$_2$	Adsorption	10	3	[56]
	SH@SiO$_2$/Cu(BTC)$_2$	210 Hb(II)	n/d	Adsorption	60	5.5	[63]
	AMOF-1	78 Hg(II)	n/d	ion exchange	1440	–	[34]
	MOF-74-Zn	63 Hg(II)	Hg(NO$_3$)$_2$	Adsorption	90	6	[66]
	MIL-101-Thymine	52 Hg(II)	HgCl$_2$	Adsorption	200	6	[64]
	ZIF-90-SH	22 Hg(II)	HgCl$_2$	Adsorption	1440	–	[62]
	Zr-DMBD	100% Hg(II)	Hg(NO$_3$)$_2$; HgCl$_2$	Adsorption	720	–	[60]
	Cr-MIL-101-AS	99% Hg(II)	n/d	Adsorption	360	–	[59]
	3D Co(II) MOF or (1)	70% Hg(II)	Hg(NO$_3$)$_2$	Adsorption	100	6	[37]
	PCN-100	1.4 Hg(II) per formula (ICP)	HgCl$_2$	Adsorption	2880	–	[35]
Others							
Al	3D Co(II) MOF or (1)	90% Al(III)	AlCl$_3$	Adsorption	100	6	[37]
Fe	3D Co(II) MOF or (1)	100% Fe(III)	FeCl$_3$	Adsorption	80	6	[37]
	Cu-terephthalate MOF	115 Fe(III)	Fe salt/Sungun wastewater	Adsorption/ion exchange	120	7	[40]
Mn	Cu-terephthalate MOF	175 Mn(II)	Mn salt/Sungun	Adsorption/ion	120	7	[40]

Table 2 (*continued*)

| Metal	MOF	Adsorption capacity (mg g^{-1}) of M ion	Metal ion source	Method	Time to adsorption equilibrium (min)	Optimal pH	Refs.
			wastewater	exchange			
Zn	Cu-terephthalate MOF	150 Zn(II)	Zn salt/Sungun wastewater	Adsorption/ion exchange	120	7	[40]
Ag	MIL-53(Al)	183 Ag(I)	AgNO$_3$	Adsorption	180	–	[67]
	HKUST-1	±100% AgNP	AgNO$_3$	Adsorption	10	6–7	[68]
Ni	Chitosan-MOF	60 Ni(II)	Ni(NO$_3$)$_2$·6H$_2$O	Adsorption	480	5	[43]
Co	TMU-5	63 Co(II)	Co(NO$_3$)$_2$·6H$_2$O	Adsorption	15	10	[39]
Cu	ZIF-8	800 Cu(II)	Cu(NO$_3$)$_2$	Adsorption/ion exchange	30	4	[73]
	MOF-5	290 Cu(II)	n/d	Adsorption	30	5.2	[69]
	Cu-terephthalate MOF	225 Cu(II)	Cu salt/Sungun wastewater	Adsorption/ion exchange	120	7	[40]
	Cd-MOF-74	190 Cu(II)	Cu(NO$_3$)$_2$	ion exchange	10	6.7	[70]
	TMU-5	57 Cu(II)	Cu(NO$_3$)$_2$·3H$_2$O	Adsorption	15	10	[39]
	Chitosan-MOF	51 Cu(II)	CuSO$_4$·5H$_2$O	Adsorption	480	5	[43]
	UiO-66(Zr)-2COOH	11 Cu(II)	Cu(NO$_3$)$_2$·3H$_2$O	Adsorption	60	6	[71]
	Dy(BTC)(H$_2$O)(DMF)$_{1.1}$	5 Cu(II)	Cu(NO$_3$)$_2$·3H$_2$O	Adsorption	10	6.5	[51]
	ZIF-8	3.5 mmol/g Cu(II)	CuCl$_2$·2H$_2$O	Adsorption	20	–	[72]
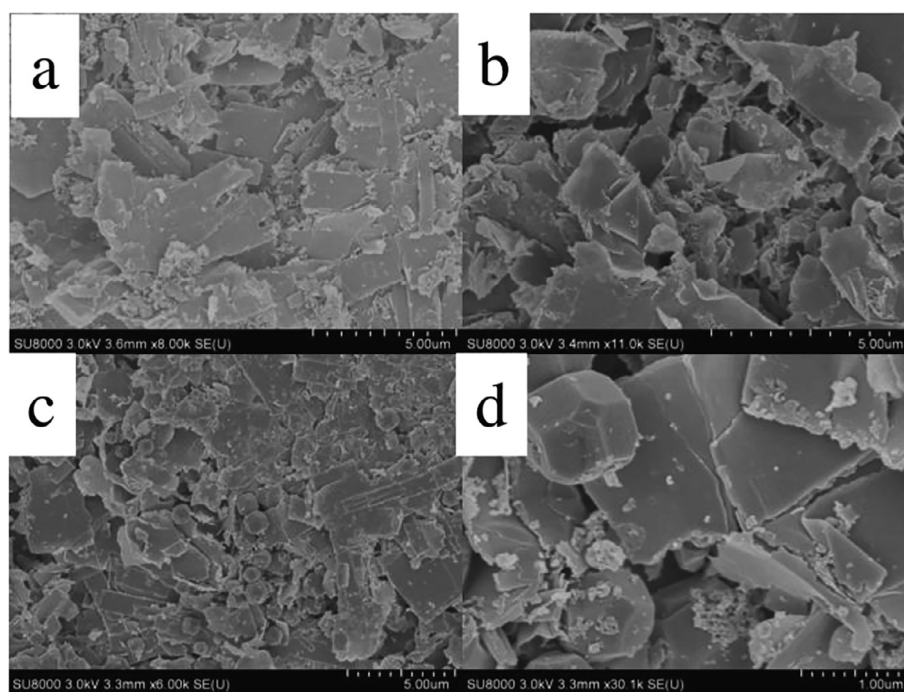
Fig. 2. A set of SEM images showing the spent adsorbents: cubic (a), leaf-shaped (b) and dodecahedral (c) and (d). Reproduced with permission from Ref. [26].

2015, Wang et al. reported the adsorption of As(V) in **UiO-66** (Fig. 3 (a) and (b)) with an unprecedented capacity of 303 mg g^{-1} at an optimal pH of 2. The MOF also displayed promising adsorption capacity across a broad pH range (pH 1–10). The arsenic ion uptake was also found to be mostly unaffected by other anions present in the solution. X-ray powder diffraction (PXRD) and FT-IR spectroscopy suggest the adsorption mechanism occurs via coordination at either the hydroxyl groups on the Zr node (Fig. 3(c)) or by replacement of the BDC ligands (Fig. 3(d)) in the framework. The study found that at equilibrium one Zr$_6$ cluster could adsorb seven arsenic species [30]. Finally in 2016, Audu et al. described the dual capture of As(III) and As(V) species (As$_2$O$_3$ and Na$_2$HAsO$_4$·7H$_2$O respectively) using the thiolated derivative of UiO-66, UiO-66-(SH)$_2$. In this example the As(V) species were found to interact with the MOF node while the As(III) species were captured by the thiolated linker with uptake of 40 mg/g and 10 mg/g respectively after 6 h [31].

2.2. Cadmium

Wang et al. reported in 2015 the Cu$_3$(BTC)$_2$-SO$_3$H framework as an effective cadmium(II) adsorbent. The framework was synthesized via the sequential post-synthetic modification and oxidation of Cu$_3$(BTC)$_2$ with sulfonic acid. The optimal pH value for Cd(II) uptake was found to be 6. Below that value (especially below pH 3) active sites were increasingly occupied by protons, limiting adsorption, while at pH greater than 6, cadmium ions precipitated in the form of hydroxide salts. It was suggested that the adsorption
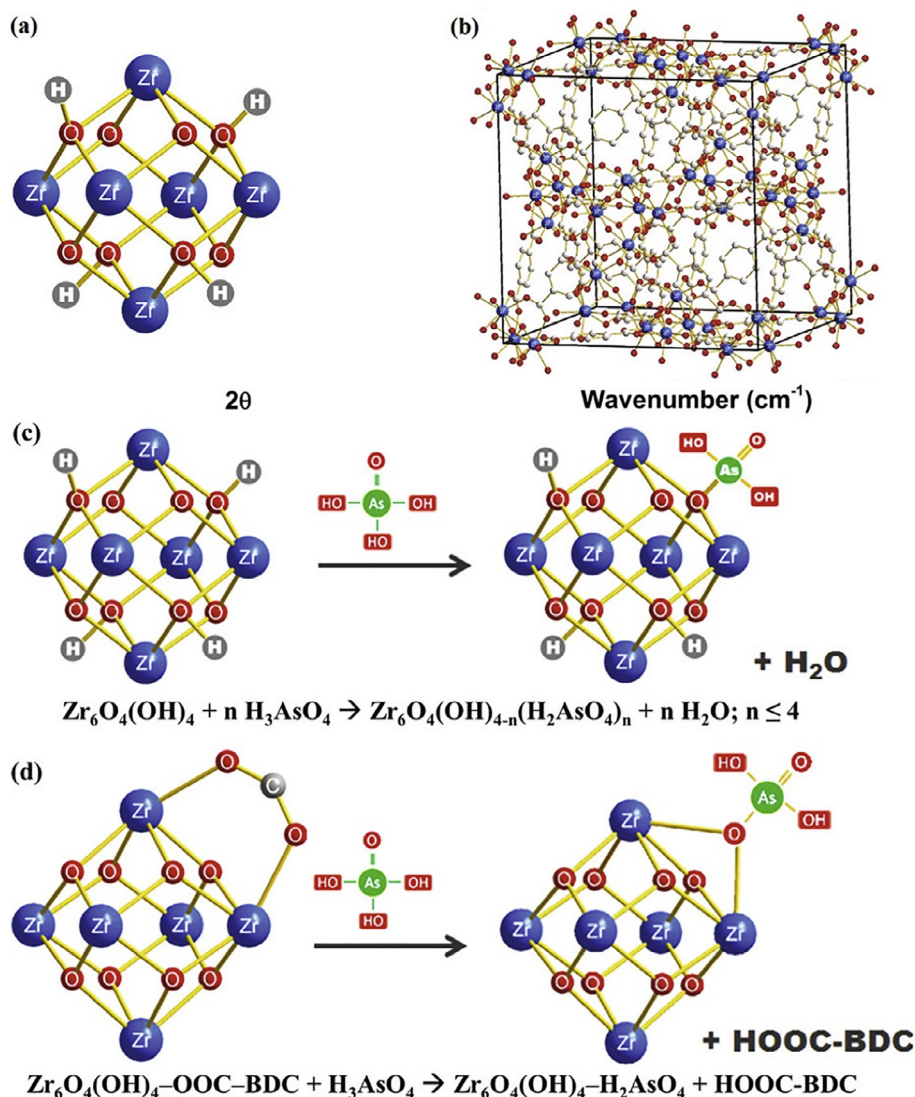
Fig. 3. A color-coded illustration of the octahedral zirconium cluster (a) and 3D unit cell of UiO-66 framework (b), as well as the adsorption mechanism for arsenate *via* coordination at either hydroxyl group site (c) or by replacement of a BDC ligand (d). Reproduced with permission from Ref. [30].
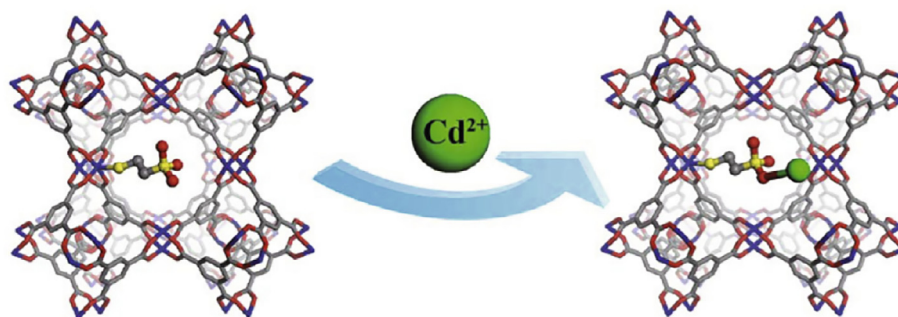

Fig. 4. Cadmium(II) adsorption mechanism onto the $Cu_3(BTC)_2$-SO_3H MOF. Reproduced from Ref. [32] with permission from The Royal Society of Chemistry.

process occurred *via* chelation between cadmium(II) and sulfonic groups of the MOF (Fig. 4).

Although a reduction in porosity of the MOF was noted with subsequent use, an easy regeneration method was proposed (washing with deionized water and drying). The sulfonic acid functionalization of the framework also led to improved selectivity for Cd(II) over other metal ions possibly due to multiple bonding sites and coordination modes of the SO_3H^- group [32].

In 2015, **AMOF-1** was synthesized by Chakraborty et al. and reported to be a possible cadmium(II) adsorbent. This material was based on zinc(II) metal ions, which were combined with flexible tetracarboxylate linkers. The maximum uptake for cadmium ions was found to be 41 mg g^{-1}, after 24-h which is when equilibrium was reached. AMOF-1 has also shown selectivity in uptake toward Cd(II) ions, albeit not complete, with other metal ions being adsorbed at roughly half the capacity [33]. Another cadmium(II)
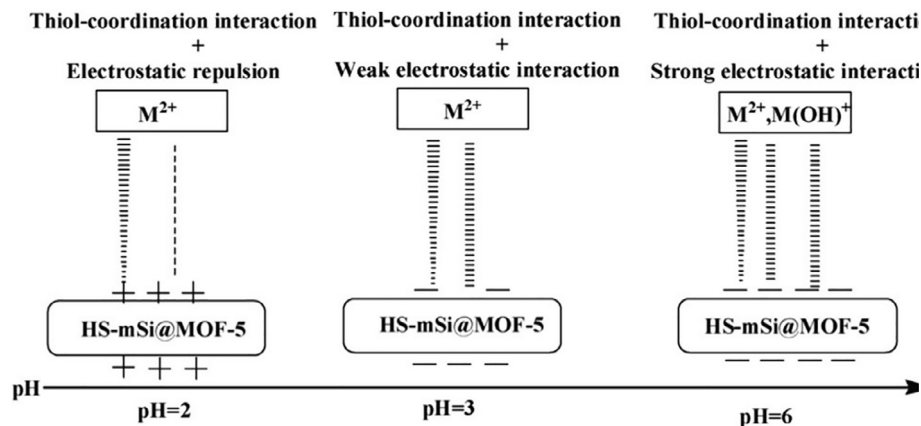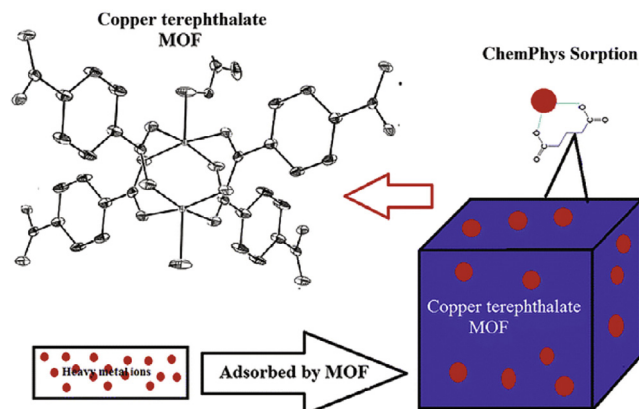
Fig. 5. Adsorption mechanism of Cd(II) and Pb(II) at different pH over HS-mSi@MOF-5 substrate showing that at higher pH the negative charge on surface facilitates the adsorption efficiency. Reproduced with permission from Ref. [37].
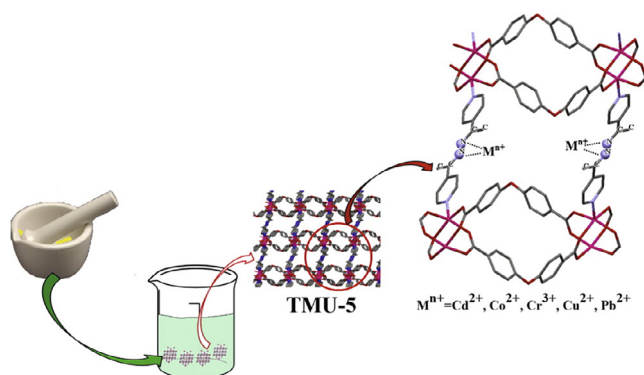

Fig. 6. Synthesis and adsorption locations of the TMU-5 framework. Reprinted with permission from Ref. [38]. Copyright 2014 American Chemical Society.

removing MOF – **PCN-100** – was presented in 2010 by Fang et al., constructed from TATAB linkers (i.e. 4,4′,4″-s-triazine-1,3,5-triyl tri-p-aminobenzoate) and $Zn_4O(CO_2)_6$ SBUs (secondary building units). The MOF was found to exhibit a chelating coordination mode through the linkers by which metal ions were encapsulated. The cadmium(II) adsorption was recorded by ICP analysis, and indicated an uptake of 1.6Cd(II) per formula unit [34]. In 2015, Saleem et al. reported on **UiO-66-NHC(S)NHMe** – a MOF able to adsorb, among other ions, cadmium(II) with maximum capacity
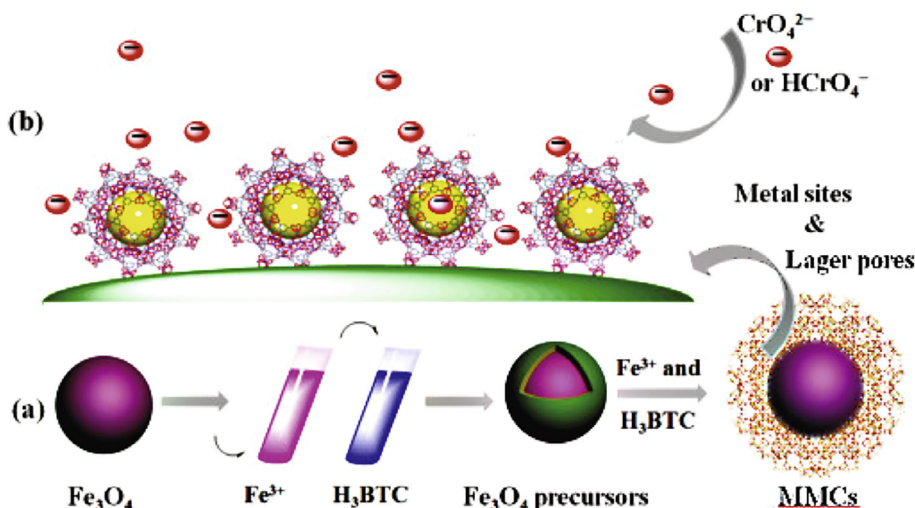
of 49 mg g^{-1} [35]. Abbasi et al. offered another MOF for Cd(II) removal in 2015 – a 3D cobalt and TATAB (TATAB = 4,4′,4″-s-triazine-1,3,5-triyltri-p-aminobenzoate) based MOF (**3D Co(II) MOF**), which was obtained *via* hydrothermal synthesis or ultrasound irradiation to give nanosized particles. A comparison between **3D Co(II) MOF** and its nanostructured version, revealed the latter to have better adsorption capacities, while the optimal pH for each sample was about 6. The lack of adsorption in acidic environments was suggested to be caused by a lack of available active —NH groups. PXRD analysis suggested the crystallinity of the material remained intact over the course of adsorption as no significant signs of deterioration were found after examination of the spent material [36]. Another framework able to remove cadmium(II) from water was presented by Zhang et al. in 2016. **HS-mSi@MOF-5** – a post-synthetically modified version of the zinc-based MOF-5 was synthesized using a hydrothermal method. The time at which HS-mSi@MOF-5 reached equilibrium for Cd(II) adsorption was
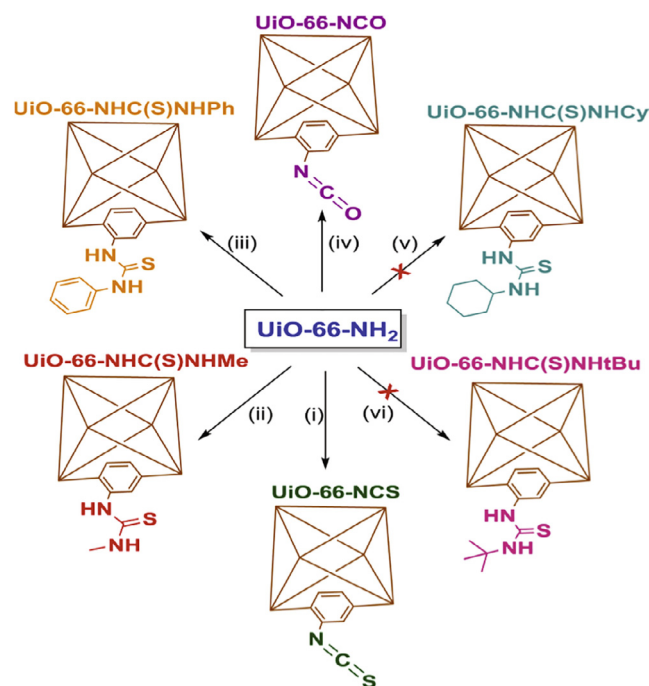
Fig. 8. Schematic showing attempted functionalization by post-synthetic modification of UiO-66-NH$_2$ using (i) CSCl$_2$, (ii) CH$_3$NCS, (iii) C$_6$H$_5$NCS, (iv) ClCOOCCl$_3$, (v) C$_6$H$_{11}$NCS, and (vi) (CH$_3$)$_3$CNCS. Reproduced with permission from Ref. [35].

Fig. 7. Illustration of the heavy metal ion adsorption process using the copper terephthalate MOF. Reproduced with permission from Ref. [39].

Fig. 9. An illustration of (a) synthesis of the Fe_3O_4@MIL-100Fe magnetic microspheres and (b) adsorption process of chromium(VI) onto the microspheres. Reproduced with permission from Ref. [41].

found to be approximately 30 min (like MOF-5), with an adsorption capacity strikingly higher than that of MOF-5 and estimated to be 98 mg g^{-1} (compared with 43.6 mg g^{-1} for MOF-5). A suggested adsorption mechanism for the metal ions in the MOF is shown in Fig. 5 [37].

Tahmasebi et al. showed in 2014, that the azine-functionalized **TMU-5** MOF was a good cadmium(II) adsorbent (Fig. 6). Here, the maximum adsorption capacity was recorded to be 43 mg g^{-1}, with a short equilibrium time of 15 min. The high optimal pH of 10 was proposed to be due to protons occupying the donor atoms (N or O) of the sorbent at lower pH [38]. In 2015, Rahimi and Mohaghegh evaluated the cadmium ion adsorption capabilities of the magnetic **Cu-terephthalate MOF** – a copper-based material, synthesized *via* solvothermal methods. The removal of metal ions occurs *via* a chemical adsorption process (as illustrated by Fig. 7), which is greatly boosted by the readily available carboxylate groups present within the MOF. Increasing the solution pH was found to aid in the metal ion removal process, as the increasingly anionic MOF surface would produce stronger electrostatic interactions with the metal ions. The maximum Cd(II) removal capacity of this MOF was found to be 100 mg g^{-1} [39]. In 2013, Zou et al. presented a novel synthesis method for the HKUST-1-MW MOF, as well as the more stable, polyoxometalate-modified version – **HKUST-1-MW@H$_3$PW$_{12}$O$_{40}$.** It was proposed that the extra stability was gained due to the MOF pores being filled by the Keggin polyoxometalate. The MOF was synthesized using microwave irradiation, where during the synthesis the polyoxometalate was introduced. The removal of Cd(II) occurred *via* chemical adsorption and the capacity of the framework was found to be 32 mg g^{-1}, with the equilibrium being reached within 80 min. Higher capacity was noticed with increasing initial metal ion concentration (up to the saturation point). Additionally, an increase in temperature seemed to improve adsorption in the studied range of 273–323 K [40].

2.3. Chromium

In 2015, Saleem et al. reported on a set of post-synthetically modified MOFs (Fig. 8) and their possible usage for chromium(III) removal from water. The most promising out of the MOFs synthesized was **UiO-66-NHC(S)NHMe** – an S-functionalized UiO-66-NH$_2$ framework, characterized by high pH and water stability. UiO-66 was reacted with a series of diphosgene/thiophosgene or isothiocyanates, thus forming a set of novel, modified MOFs. UiO-66-

NHC(S)NHMe displayed up to 25-fold improved metal ion adsorption capacity compared with the un-modified MOF [35]. Another type of chromium adsorbing MOF was introduced by Tahmasebi et al. in 2014. Here, a group of three azine- and imine-functionalized MOFs (TMU-4, 5 and 6) were synthesized *via* a mechanochemical reaction. The study focused on **TMU-5** and its metal ion removing capabilities. The MOF showed a highly ordered, three-dimensional structure of linked pores lined with azine groups. An increase in Cr(III) adsorption capacity was seen with increasing pH, with a cut-off at pH 10, at which point a sharp drop was noted with the maximum adsorption capacity originally recorded at 123 mg g^{-1} (Fig. 6) [38]. In 2016, Yang et al. documented the use of **Fe$_3$O$_4$@MIL-100Fe** magnetic microspheres for the removal of chromium(IV) ions from water. Fe$_3$O$_4$ crystal seeds were used to grow the MOF shell *in situ* (*via* hydrothermal reaction), on which the composite was based (Fig. 9). The maximum adsorption capacity of the material was noted at 18 mg g^{-1}, at an optimal pH of 2. Such acidic conditions were found to facilitate electrostatic interactions between the adsorbent (Fe$_3$O$^+$) and chromium ions (HCrO$_4^-$) and so adsorption decreased with increasing pH (minimum adsorption capacities found at neutral pH). The microspheres were characterized by rapid metal ion uptake, where adsorption equilibrium was reached after 2 h [41]. A **chitosan-MOF (UiO-66) composite**, able to adsorb 94 mg g^{-1} of chromium (VI) (in the form of Cr$_2$O$_7^{2-}$), was reported in 2016 by Wang et al. The adsorption values were found to be higher than that for chitosan itself. The composite was synthesized by grinding and microwave irradiation. Here, Cr(VI) adsorption capacities were high due to the strong electrostatic attraction between high oxidation state metal ions and oxygen atoms or the —NH$_2$ groups of the linkers. Such capacities were prevalent at lower pH values, whereas increasing the basicity of the solution led to decreased adsorption caused by —OH groups blocking the active sites [42]. Maleki et al. reported another Cr-adsorbing MOF in 2015. It was **Cu-BTC**, a copper-benzenetricarboxylate based MOF.

The adsorption capacity for Cr(VI) (in the form of Cr$_2$O$_7^{2-}$) was found to be 48 mg g^{-1}. It was shown that the maximum adsorption occurred at a solution pH of about 7 [43]. A silver-triazolato MOF – **1-NO$_3$** – was reported in 2016 by Li et al. Its chromium (VI) adsorption (in the form of Cr$_2$O$_7^{2-}$) was based on an ion exchange mechanism. The adsorption of chromium was moderate and reached equilibrium at about 4 h (Fig. 10). The MOF was found to be reusable, as after four consecutive adsorption-release cycles,
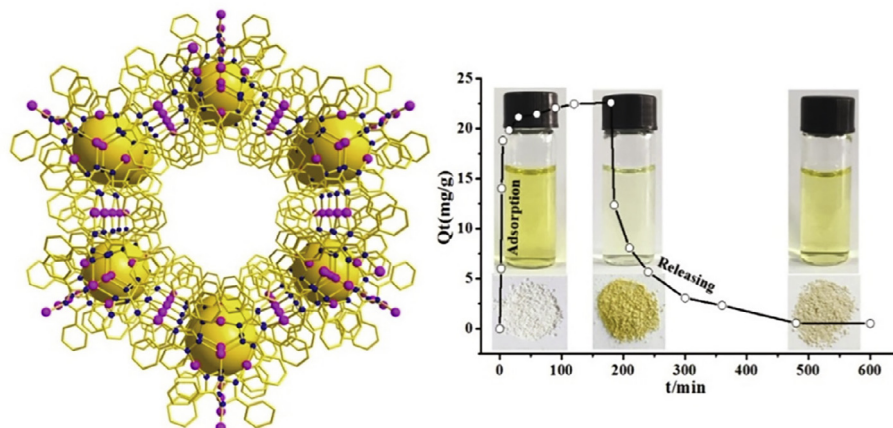
Fig. 10. A 3D rendering of 1-NO_3 along with its Cr(VI) adsorption and release values set against time. Reproduced with permission from Ref. [44].
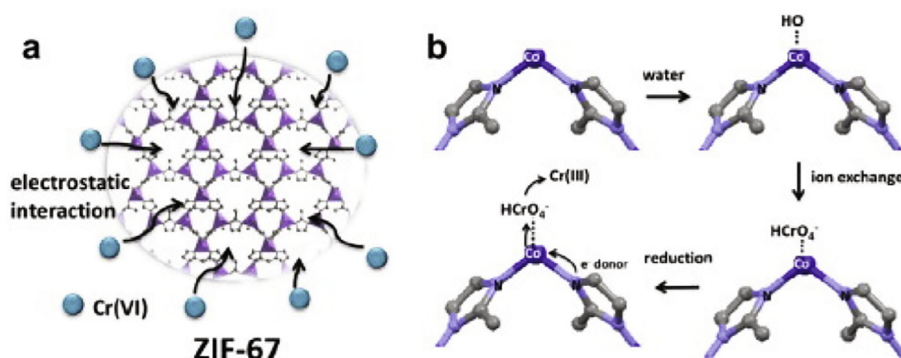

Fig. 11. An illustration of the electrostatic interaction (a) and ion exchange (b) adsorption mechanisms of ZIF-67 for chromium(VI) removal. Reproduced with permission from Ref. [46].

the material retained 93% of its original effectiveness. 1-NO_3 also displayed a preference for $Cr_2O_7^{2-}$ adsorption over other anions, such as SO_4^{2-}, NO_3^-, ClO_4^- or Cl^- [44]. In 2015, Zheng et al. designed a cationic, zirconium-based MOF, **ZJU-101**, with unprecedented chromium(VI) adsorption capabilities (245 mg g^{-1}). The MOF was created by performing a post-synthetic modification of MOF-867, to which methyl groups were added. The adsorption equilibrium was reached after only 10 min, with a 96% $Cr_2O_7^{2-}$ concentration reduction within the solution (50 ppm initial concentration). The initial adsorption capacity of ZJU-101 was found to be 324 times higher than that of its precursor, MOF-867. ZJU-101 also had excellent adsorption selectivity for $Cr_2O_7^{2-}$ over other anions (SO_4^{2-}, NO^{3-}, Cl^-, Br^-, I^- or F^-) [45].
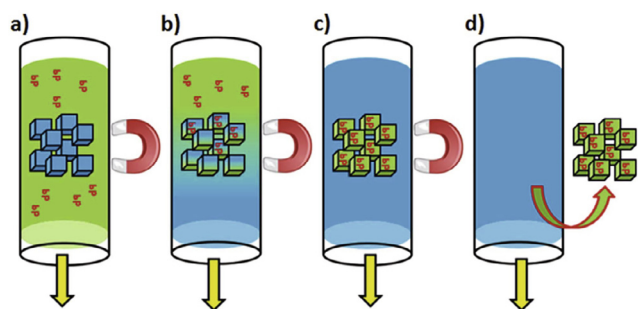
In 2015, Li et al. studied the chromium(VI) adsorption properties of the cobalt-based zeolitic imidazolate framework-67 (**ZIF-67**). The adsorption equilibrium was reached faster at lower starting concentrations and the adsorption capacity was found to increase slowly with contact time after the initial fast uptake period. It was proposed that the adsorption mechanism was ion exchange (Fig. 11) between the chromium(VI) anions ($Cr_2O_7^{2-}$) and the hydroxyl groups of the MOF, which agreed with the observation of increasing pH during the adsorption process (from pH 76.5 to 9 in 3 h). The adsorption process was also found to be promoted by electrostatic interactions between the MOF crystals and chromium(VI) anions at low pH values (adsorption capacity increasing as pH decreases, moving away from the point zero charge of the MOF, located at pH of 9) [46]. Additionally, in 2016 Aboutorabi et al. synthesized **TMU-30** – an isonicotinate N-oxide based MOF for effective chromium(VI) removal (in the form of CrO_4^{2-}) from water. This framework, consisting of 1D rhombic tunnels, was highly effective at Cr(VI) removal (145

mg g^{-1}) within a short time (equilibrium reached within 10 min) and over an extremely wide solution pH range (between 2 and 9). Per PXRD analysis, adsorption at such a wide pH range was found to have little to no effect on the crystalline structure of the MOF, with the first signs of structural change occurring at pH above 9. Adsorption selectivity tests showed that TMU-30 adsorbed CrO_4^{2-} over other ions (with rare exceptions such as MoO_4^{2-} or WO_4^{2-}) [47]. Finally, Rapti et al. reported in 2016 a green, fast and safe synthesis method for **MOR-1-HA**; a UiO-66 based, amino-functionalized MOF with an alginic acid coating. MOR-1-HA was created via reflux synthesis. The adsorption of Cr(VI) occurs via an ion exchange mechanism, where Cl^- anions of the MOF are exchanged with $Cr_2O_7^{2-}$ from the solution. The maximum adsorption capacity was calculated to be near 280 mg g^{-1}, which was lower than that found for the unmodified MOR-1. This led to the conclusion that the alginic acid coating alters ion exchange capabilities of the MOF. Varying the solution pH did not significantly alter the adsorption capability of the MOF between pH 2 and 8, while at pH 1 a noticeable drop was observed. Other anions were found to have very little influence on $Cr_2O_7^{2-}$ adsorption, even in the presence of a ten-fold excess of SO_4^{2-} [48]. In addition to the conventional approaches there have been recent progresses in photocatalytic reduction and separation of Cr(VI) ions using MOFs, and this topic has been reported in a recent review [49].

2.4. Lead

Saleem et al. reported in 2015 on the ability to use the zirconium-based MOF, **UiO-66-NHC(S)NHMe**, as an effective adsorbent for lead(II). The maximum adsorption capacity was

reported at 232 mg g^{-1} for lead(II) [35]. Abbasi et al. introduced **3D Co(II) MOF** for the removal of lead ions from water. The findings showed adsorption values to be closely related to solution pH (optimal pH is 6), the concentration of the metal ions and exposure time (equilibrium reported to be reached at about 100 min) but no information on capacity was given [36]. Another MOF, a silica-coated, thiolated MOF-5 derivative, **HS-mSi@MOF-5**, was tested for Pb(II) removal by Zhang et al. in 2016. The high adsorption capacity of this material (312 mg g^{-1}), as well as the time at which equilibrium is reached (about 30 min) make this an effective adsorbent. The adsorption process is aided greatly by increasing the pH of the solution. At lower pH the acidic conditions promote competition between the metal ions and a proton whereas increasing the solution pH above 6, lead to precipitate formation within the solution. Hence, the optimal pH for Pb(II) adsorption in HS-mSi@MOF-5 was 6. A detailed illustration of the effects of pH on the adsorption process can be seen in Fig. 5 [37]. Another Pb(II) adsorbing MOF was reported by Tahmasebi et al. in 2014. Here, the mechanochemically prepared TMU-5 (Fig. 6) with azine-functionalized pores was shown to be an effective lead(II) adsorbent. The maximum adsorption capacity was reported to be 251 mg g^{-1}, with equilibrium being reached after only 15 min. Low solution pH was found to lower the adsorption capacity of the MOF due to active sites of the sorbent being protonated, the optimal pH for the procedure was therefore set at 10 [38]. In 2015, Ricco et al. prepared a group of magnetic framework composites **MIL-53(Al@100aBDC)** based on a combination of MIL-53 with iron oxide nanoparticles. The number of amino groups, introduced via 1,4-benzenedicarboxylic acid (H$_2$BDC) and 2-amino-1,4-benzenedicarboxylic acid (H$_2$aBDC) within the MOF was varied using modified synthetic conditions to give 0%, 50% and 100% amino group-loaded material. The presence of 50% or more —NH$_2$ moieties was found to lead to a significant increase in lead(II) uptake by the MOF. The maximum uptake capacity was recorded at 492 mg g^{-1}, while the equilibrium was reached after six hours without heating (two hours when heating was applied). A theoretical removal method employing this MOF is presented in Fig. 12 [50]. Yet another framework capable of removing lead(II) ions from water was introduced by Chakraborty et al. in 2016. This zinc(II) and tetracarboxylate based, anionic MOF (**AMOF-1**) was recorded to have a maximum lead ion uptake of 71 mg g^{-1}, with the equilibrium being reached within 24 h [33]. In 2015, Rahimi and Mohaghegh assessed the lead ion uptake in **Cu-terephthalate MOF** (Fig. 7). With the optimal pH set at 7, the maximum uptake capacity was recorded at around 80 mg g^{-1}, while the equilibrium was reached after 120 min [39]. Furthermore, in 2013, Zou et al. reported on an efficient synthesis method for HKUST-1, and its subsequent functionalization with a polyoxometalate to give

HKUST-1-MW@H$_3$PW$_{12}$O$_{40}$ – a framework with promising selectivity and uptake for lead(II) ions. Its maximum adsorption was recorded at 98 mg g^{-1}, with only a short time required to reach equilibrium (10 min) [40]. Another framework capable of removing lead(II) from water was reported by Jamali et al. in 2016. This lanthanide-based, rod-like MOF – **Dy(BTC)(H$_2$O)(DMF)$_{1.1}$** – exhibited moderate uptake values (5 mg g^{-1} of Pb(II)), while being able to achieve equilibrium within only 10 min. As the framework would protonate at lower solution pH, it was found that higher pH values had a positive effect on the metal ion uptake. The optimal pH was therefore set at 7. The MOF was also found to be reusable, where after 5 consecutive cycles it would retain 94–98% of its adsorption capacity [51]. In 2011, **MnO$_2$-MOF** was proposed by Qin et al. to be an extremely effective lead(II) ion adsorbent in aqueous solutions. The material was synthesized *via* oxidation of MnSO$_4$ by KMnO$_4$. The metal ion uptake of this MOF was characterized by fast equilibration (within 1 h) and an unprecedented uptake capacity for lead(II) ions, recorded at 917 mg g^{-1}. The initial solution pH of 6 dropped to 5 during the uptake process, which was attributed to proton release during the adsorption process. The overall reaction mechanism was suggested to be driven by inner-sphere complexation of the MOF sites (hydroxyl groups) with the metal ions [52]. Lastly, in 2016, Rivera et al. showed that **MOF-5** also presents excellent lead(II) uptake from water, with a maximum capacity calculated to reach 659 mg g^{-1} at 45 °C. The uptake value was found to fluctuate with changing temperature, with no constant increase/decrease trends. Due to the structure of this MOF, which has both acidic and basic active sites, the uptake value (recorded at 450 mg g^{-1} at pH 5) increases with both increasing and decreasing pH to 750 mg g^{-1} at pH 4 and 660 mg g^{-1} at pH 6 [53].

2.5. Mercury

In 2011, Ke et al. reported on the synthesis of a post-synthetically modified HKUST-1 MOF, **Thiol-HKUST-1**, and its mercury(II) ion adsorption properties. While the base framework was synthesized by a solvothermal method, the thiol functionalization was added by treatment with dithioglycol onto the sites previously occupied by coordinated water molecules (Fig. 13). SEM analysis revealed the functionalized MOFs to have a rough but still octahedral structure. Furthermore, EDX spectra revealed that control of the amount of thiol sites is possible with molar ratio adjustments of the dithioglycol:MOF. Interestingly, while the unmodified HKUST-1 MOF exhibited no affinity toward mercury(II) ions, the thiol modified version exhibited exceedingly good adsorption values (714 mg g^{-1}, almost 100% removal rate) from water, with equilibrium being reached within the first 120 min. The high uptake was attributed toward the large specific surface area and quantity
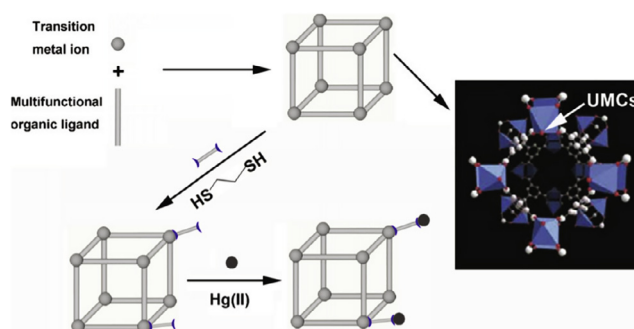

Fig. 12. A schematic of a proposed system for heavy metal removal from polluted water using MIL-53(Al@100aBDC) and a magnetic field, with pollutants passing through a MOF sieve (a) and being trapped by it (b) and (c), after which magnetic field is removed (d) and adsorbed metal ions separated from now purified water. Reproduced from Ref. [50] with permission from The Royal Society of Chemistry.


Fig. 13. An illustration of the functionalization process of Thiol-HKUST-1 with thiol groups being grafted onto the unsaturated metal centers (denoted as UMCs). Reproduced with permission from Ref. [54].

of functionalized adsorption sites within the pores of this MOF [54]. Subsequently, **UiO-66-NHC(S)NHMe** was synthesized by Saleem et al. in 2015 by performing covalent post-synthetic modifications on the base UiO-66-NH$_2$. The Hg(II) adsorption properties of this MOF were tested and a substantial increase (up to 25-fold) in metal ion uptake was noted for the modified framework, with adsorption reaching 99% after 240 min for a solution with 100 mg L^{-1} of target metal ion. UiO-66 alone exhibited very little affinity toward mercury ions, where adsorption was only 4% [35]. Next, adsorption properties of mercury(II) in water were investigated by Abbasi et al. in 2015, where they examined a 3D **Co(II) MOF** as a possible adsorbent. The study was performed with various concentrations (10 ppm, 20 ppm, 30 ppm and 40 ppm of Hg(II)) prepared by dilution of an aqueous stock solution of Hg(NO$_3$)$_2$. The MOF was found to adsorb 70% of the Hg(II) in solution, with equilibrium being reached within 100 min at an optimal pH of 6. PXRD analysis revealed no significant damage to the MOF structure after use [36]. In 2016, Liang et al. developed another novel, sulfur modified MOF – **FJI-H12** – and presented its mercury(II) uptake capabilities. This novel framework, synthesized under mild conditions, consisted of free NCS$^-$ groups located within octahedral M$_6$L$_4$ cages (built from Co(II) metal ions and 2,4,6-tri(1-imidazolyl)-1,3,5-triazine linkers). It was suggested, that the uptake mechanism relies – to a varying degree – on both chemisorption and physisorption, where both coordination and adsorption are directed by the SCN$^-$ groups. The maximum uptake capacity was calculated to be 440 mg g^{-1} with the adsorption rate visibly slowing down after 1 h. The optimal pH was set at 7, however no adsorption increase was noted with pH being increased from 3 to 6. The regeneration of the MOF was achieved by immersion in KSCN solution over a 24 h period (where 86% of the material was recovered). The effectiveness of the adsorbent was, however, reduced during subsequent tests [55]. Also, Fang et al. reported in 2010 on a newly synthesized **PCN-100** and its Hg(II) adsorption in aqueous solutions. This zinc-based framework employs TATAB as a linker and the framework pore

Fig. 14. A rendering of Zn(hip)(L)·(DMF)(H$_2$O) metal–organic framework, as seen from above (along the *c*-axis) and as a labeled cross section along the main channel's length. Reproduced from Ref. [57] with permission from The Royal Society of Chemistry.

have chelating coordination modes, not unlike aminopyridinato complexes. Upon adsorption experiments (conducted in DMF solution), ICP analysis of the framework found that impregnation of 1.38 Hg(II) per formula occurred [34].

Following this, in 2015 Chakraborty et al. synthesized a new MOF based on zinc metal ions and tetracarboxylate linkers – **AMOF-1** – and tested the MOF for removal of mercury ions from water. A series of time-dependant experiments showed that AMOF-1 could adsorb 94% of mercury(II) (initial concentration 1 ppm) ions within the first 18 h, whereas doubling this time allowed the adsorption rate to increase to 99%. The calculated maximum uptake capacity of this material was 78 mg g^{-1}, however no pH values were provided. The proposed adsorption mechanism was based on ion exchange with the DMA ligands located within the rectangular MOF channels [33]. A magnetic MOF – **Fe$_3$O$_4$@-SiO$_2$@HKUST-1** – was introduced by Huang et al. in 2015 and its mercury(II) water-based adsorption was tested. The MOF is based on the post-synthetic functionalization of HKUST-1 with bismuthiol (Bi-I). The material was found to have promising kinetics for mercury(II) adsorption, with equilibrium being reached within 10 min. The maximum uptake capacity was found to be 264 mg g^{-1} corresponding to 99% adsorption from a solution with concentration 20 mg L^{-1}. The framework was also found to be highly selective, wherein exposure to other metal ions at the same concentrations led to only 23% uptake of lead(II) ions and 55% of chromium(III) ions. The MOF exhibited a somewhat constant adsorption value across a range of pH from 2 to 9 with an optimal value of 3 [56]. **Zn(hip)(L)·(DMF)(H$_2$O)** – another newly designed MOF was introduced by Luo et al. in 2015 as an efficient adsorbent for mercury(II) from water. The material was created using a solvo(hydro)thermal method. As can be seen in Fig. 14, the structure of this MOF displays a single, hexagonal channel equipped with hydroxyl and acylamide active sites along the inner pore walls. The maximum adsorption capacity was calculated to be 333 mg g^{-1}, with equilibrium occurring within 1 h. The efficiency of this MOF was tested across a range of pH values and it was found that the uptake peaked at pH 5, while decreasing under both acidic and basic conditions. Also, the framework was found to work at ultra-low mercury(II) concentrations as low as 5, 10 and 20 ppb with removal of 71%, 83% and 85% of the Hg(II) respectively [57]. In 2017, Halder et al. proposed to use **[Ni(3-bpd)$_2$(NCS)$_2$]$_n$** for mercury(II) removal from aqueous solutions. Here, the key functionality making Hg ion adsorption possible is bond formation between the uncoordinated sulfur atom of the bridging thiocyanato ligands and the metal ions. This affinity for mercury was confirmed, when the MOF, exposed to several metal ions, would selectively coordinate only to Hg(II). Interestingly the MOF changes color from green to gray when adsorption of mercury occurs, allowing for naked-eye mercury ion detection in solution. The MOF also exhibits extremely high selectivity toward mercury ions over other metals i.e., Pb^{2+}, Cd^{2+}, As^{3+} and Ag$^+$ (as confirmed by UV–vis spectra). The maximum adsorption capacity was estimated to be 713 mg g^{-1}, corresponding to 94% removal from a solution with concentration 10 μg L^{-1} and the equilibrium was reached within 2 h [58]. In 2014, Liu et al. synthesized a group of novel, post-synthetically modified frameworks, wherein **Cr-MIL-101-AS** was proposed as an effective mercury(II) adsorbent in aqueous solutions. Cr-MIL-101-AS was post-synthetically modified to include densely packed thiol groups (converted from the benzyl alcohol moieties of the precursor MOF) along with the already present alkenyl functions. Starting with a Hg(II) concentration of 10 ppm, 99% was adsorbed after 6 h, while a 100-fold drop of concentration (0.1 ppm) led to uptake of 93%. The material was reusable for at least two additional cycles, where no losses of adsorption capacity were noted. Neither maximum adsorption capacity, nor optimal pH values were provided [59]. Yee et al. reported in 2013 on successful application of **Zr-DMBD**
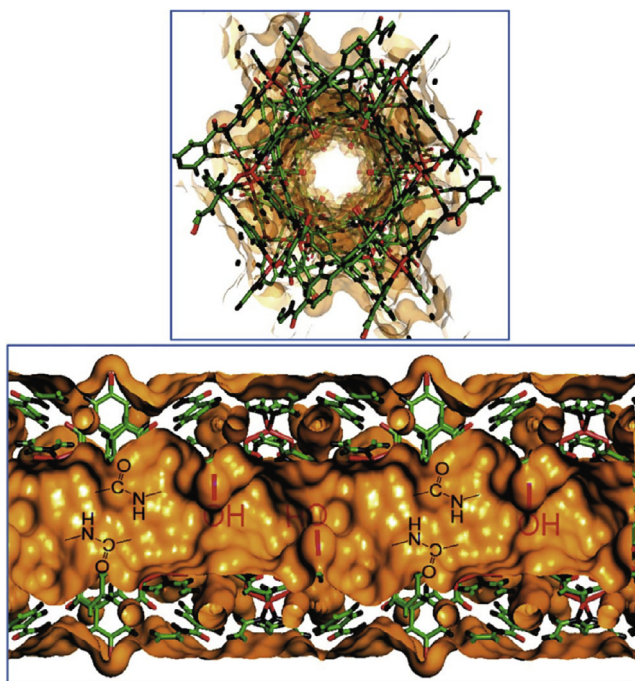
framework as a mercury(II) adsorbent from aqueous medium. This framework, based on zirconium metal ions and dimercapto-1,4-b enzenedicarboxylic acid linkers (H_2DMBD), was characterized by its structure analogous with the UiO-66 MOF, as well as by its functionalization with hard carboxyl and soft, free-standing thiol groups. Such composition allows for both presence of donor groups (soft) and complexation of metal ions (hard). The material was reported to have a promising 100% Hg(II) uptake from water (leaving the solution concentration of this ion to be below 0.01 ppm after starting with 10 ppm), with an adsorption time of 12 h. Furthermore, naked-eye detection of the adsorption process is possible due to the natural photoluminescence of the material, which is effectively quenched upon adsorption (decreased to 1/10th of its intensity) [60]. Moreover, in 2016, Rudd et al. designed **LMOF-263** – one of a series of isoreticular, luminescent MOFs, exhibiting very promising mercury adsorption capabilities. This MOF, synthesized via a solvothermal method in a mixed solvent system, incorporated functionalized, structure-modulating dicarboxylate-based ligands (dibenzo[b,d]thiophene-3,7-dicar boxylic acid 5,5-dioxide) along with tetradentate chromophores (fluorophore 1,1,2,2-tetrakis(4-(pyridine-4-yl)phenyl)ethane). The material was discovered to be a highly selective heavy metal detection tool, with mercury(II) quenching its photoluminescence in water by 84% (64% for lead ions). Its maximum adsorption capacity was estimated to be 380 mg g^{-1} and equilibrium reached within 30 min. The adsorption mechanism was found to be based around the HSAB concept, i.e., interactions between the sulfone of the MOF and acids in the solution [61]. In addition, Bhattacharjee et al. revealed in 2015 another post-synthetically modified MOF – **ZIF-90-SH** – and its ability to remove mercury ions from water at moderate rates. The material, with added thiol functionalization, was synthesized in one step. PXRD indicated that the structural integrity of the base MOF (ZIF-90) was preserved in this newly modified material. The maximum adsorption capacity of this framework was estimated to be 22 mg g^{-1}, having a varying efficiency of 45%, 75% and 90% depending on metal ion concentration in the solution (50, 30 and 25 mg L^{-1} respectively), hence, it can be said that uptake percentage is inversely proportional to mercury concentration [62]. A further study by Sohrabi, conducted in 2013, proposed the use of a **SH@SiO$_2$/Cu(BTC)$_2$** nanocomposite as a highly adsorbent mercury removal material. The composite is based on HKUST-1 and thiol-modified silica nanoparticles immobilized

within its structure. Here, the maximum adsorption capacity was calculated to be 210 mg g^{-1}, with equilibrium being reached within 60 min at an optimal pH of 6. Higher pH was detrimental due to mercury precipitation, while more acidic pH promoted active site protonation. The material was also found to be highly selective, where the presence of different metal ions in solution did not affect mercury ion uptake [63]. In 2015, Luo et al. designed a post-synthetically modified MIL-101 with thiol functional groups, **MIL-101-Thymine**, and tested the material for mercury ion adsorption in aqueous solutions. Adsorption was thought to occur due to mercury ions coordinating with two thymine groups of the MOF (Fig. 15). The maximum uptake capacity of MIL-101-Thymine was found to be 52 mg g^{-1}, with equilibrium being reached within 200 min at an optimal pH of 6. A decrease in adsorption capacity was noted for both more basic and acidic pH. The framework was found to be preferentially selective toward mercury over other light and heavy metal ions [64].

Another MOF (denoted **BioMOF**) was developed and presented in 2016 by Mon et al. as a stable mercury adsorbent, with an unprecedented uptake capacity. This newly synthesized material featured a honeycomb structure with hexagonal tunnels, functionalized with thioalkyl chains giving it exceptional affinity toward mercury ions. Its ability to adsorb mercury was investigated using $HgCl_2$ and CH_3HgCl in water and water/methanol media. The maximum adsorption capacity for $HgCl_2$ was found to be 900 mg g^{-1}, while for CH_3HgCl the value capped at 166 mg g^{-1} after 72 h. The MOF was found to be reusable, with the adsorption process reversed using dimethyl sulfide [65]. Lastly, mercury(II) adsorption from water was investigated by Xiong et al. in 2017, where they explored adsorption in **MOF-74-Zn**. The framework was synthesized by a solvo(hydro)thermal method. The adsorption mechanism was suggested as a combination of chemi- and physisorption, with adsorption thermodynamics analysis suggesting physical sorption was of greater importance. Under pH 6, the maximum adsorption capacity was calculated to be 63 mg g^{-1}, with equilibrium being reached within 90 min. As for ultra-low Hg(II) concentrations (50 ppb), a maximum uptake of 72% was observed at 45 °C [66].

2.6. Other metals

Since we have given an overview of the literature reports on heavy metal capture using MOFs, the remaining metals are included for completeness even though many of the metals that follow do not have the same toxicity issues as those discussed so far. As such, the findings described here will be listed accordingly, per report they were found in, instead of per metal ion.

In 2015, Cheng et al. successfully synthesized **MIL-53(Al)** – a MOF with reported affinity toward adsorption of silver(I) ions. The framework was created by post-synthetic modification of MIL-53 with thiol groups, which are known to coordinate strongly with heavy metals. Interestingly, an agglomeration effect was observed, where nearby adsorbed silver ions would congregate, thus creating silver nanoparticles stabilized within the framework by the thiol groups. The maximum adsorption capacity was 183 mg g^{-1}, achieved within contact time of 3 h [67].

Another Ag(I)-adsorbing framework was proposed by Conde-Gonzalez et al. in 2016, where **HKUST-1** was shown to be an effective **AgNP** (silver nanoparticle) adsorbent within aqueous medium. This material enables visual confirmation of the process, as the blue MOF, upon adsorbing the AgNP, changes color to dark green (whereas a uniform AgNP solution is yellow in color). It was found that the temperature should not exceed 50 °C, as this led to HKUST-1 becoming unstable, causing disintegration. The silver particles were found to interact with the MOF surface (rather than enter the inner pores) [68].
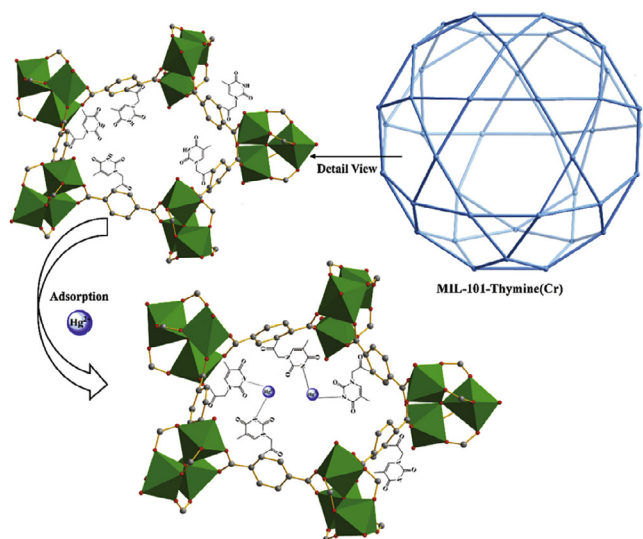

Fig. 15. A schematic illustrating the mercury(II) two-coordination with MIL-101-Thymine MOF. Reproduced with permission from Ref. [64].

In 2015, Abbasi et al. synthesized the **3D Co(II) MOF** and described its aluminum(III) and iron(III) removal capabilities from aqueous solutions. The material allowed for naked-eye adsorption detection, as it changed color upon impregnation with metal ions (for instance, a change from its original purple to yellow upon iron(III) adsorption). The MOF adsorbed 100% Fe(III) and 90% Al (III), with equilibrium being reached within 80 and 100 min and an optimal pH of 6 in both cases when studied with various concentrations of the metal ions (10 ppm, 20 ppm, 30 ppm and 40 ppm) [36].

A magnetic **Cu-terephthalate MOF** was evaluated as an effective iron(III), manganese(II) and zinc(II) adsorbent from liquid, as reported by Rahimi and Mohaghegh in 2015 (Fig. 7). Here, the maximum adsorption capacities were found to be around 175, 150 and 115 mg g^{-1} for Mn(II), Zn(II) and Fe(III) respectively, at an optimal pH of 7 and with equilibrium being reached within 120 min for all three [39].

Next, **Chitosan-MOF** was introduced as an effective nickel(II) adsorbent in water by Wang et al. in 2016. This chitosan-based MOF was synthesized using microwave irradiation. The adsorption process onto the MOF was reliant on Lewis acid–base interactions, where nickel ions (Lewis acids) would interact with the —NH$_2$ sites and oxygen atoms of the MOF (Lewis bases). Here, the maximum adsorption capacity for nickel(II) ions of 60 mg g^{-1} was obtained at pH 5 and 20 °C after 8 h [42].

Finally, in 2014, Tahmasebi et al. studied **TMU-5** as an effective cobalt(II) adsorbent. It was synthesized by mechanochemical methods and was (Fig. 6) functionalized with azine- and imine groups. Such modifications allow for Lewis acid–base interactions

between those sites and the metal ions. The maximum uptake capacity of this MOF was found to be 63 mg g^{-1}, with equilibrium occurring quickly, after only 15 min. The optimal pH for this process was set at 10, which effectively limits the protonation of donor MOF atoms (nitrogen and oxygen), allowing for higher adsorption values. Ultimately, the green synthesis method, low sorbent requirements and lack of solvent needed makes TMU-5 a promising heavy metal adsorbent [38].

The zinc(II) based MOF, **TMU-5**, reported by Tahmasebi et al. in 2014, was one of the few known MOFs reported at the time to adsorb copper ions from water. TMU-5 was synthesized using green methods and has azine-functionalized pores, able to adsorb – among others – copper(II) ions (Fig. 6). TMU-5 demonstrates a Cu(II) adsorption capacity of 57 mg g^{-1}. Notably, the other two frameworks reported – TMU-4 and TMU-6 (which weren't the focus of this research), had slightly higher copper adsorption values: 62 mg g^{-1} and 60 mg g^{-1}, respectively. The best adsorption capacities were reported at high pH (about 10), possibly due to deprotonation of the MOF donor atoms (O or N) [38]. In 2015, a magnetic **Cu-terephthalate MOF** was reported by Rahimi and Mohaghegh to be a copper(II) – and other metal ion – adsorbent. It was inferred that the relatively fast adsorption process (120 min to reach adsorption equilibrium) occurred *via* chemisorption and ion exchange at many active sites (carboxylate ligands) present on the MOF surface (Fig. 7) [39]. In 2016, Wang et al. discussed the Cu(II) adsorption capabilities of the **Chitosan-MOF** composite. This framework was rapidly synthesized using microwave irradiation and was found to be able to adsorb copper(II) with a maximum capacity of 55 mg g^{-1}. The equilibrium adsorption was
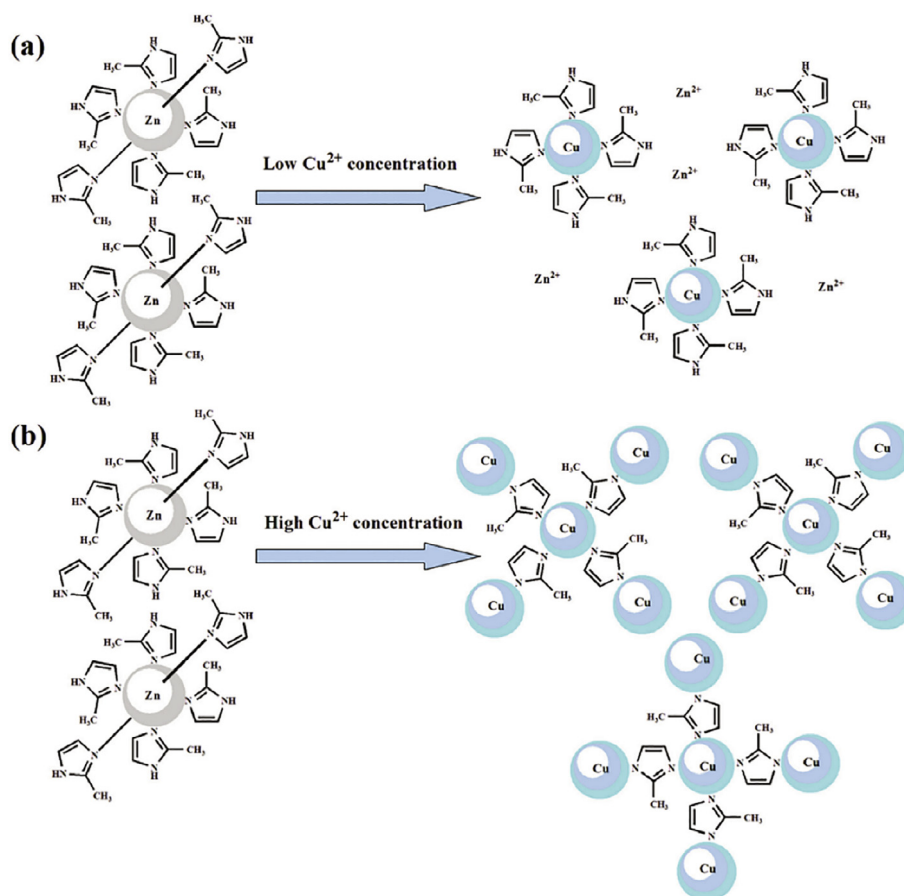
Fig. 16. The ZIF-8 adsorption mechanism for copper(II) ions at low (a) and high (b) metal ion concentrations *via* ion exchange and coordination respectively. Reproduced from Ref. [73] with permission from The Royal Society of Chemistry.

reached at 8 h and the adsorption method was found to be based on interactions between the heavy metal ions and the oxygen atoms or —NH$_2$ groups of the MOF. The effectiveness of the MOF decreased with increasing pH (optimal pH for copper adsorption was 5), attributed to a decrease in available active sites due to the interaction with other anionic molecules such as OH$^-$ [42]. In 2016, Jamali et al. presented a set of four lanthanide-based MOFs. Among them, **Dy(BTC)(H$_2$O)(DMF)$_{1.1}$** was found to have the highest copper(II) adsorption capacity. The MOF was found to perform best at neutral and basic solution pH, while increasing solution acidity caused the framework to dissolve (confirmed *via* PXRD at pH of 4). Hence, the optimal adsorption pH for Cu(II) in the framework was found to be around 7, when the activation of adsorption sites (*via* deprotonation of carboxylic acid and hydroxyl groups) occurred. After 5 cycles, recovery of the adsorbent was found to be possible [51]. In 2015, Bakhtiari and Azizian presented the zinc-based **MOF-5** as an effective copper(II) adsorbent. The framework was found to have an exceptional adsorption capacity of 290 mg g^{-1}, with equilibrium reached at 30 min. The adsorption value was found to increase with increasing temperature and the optimal pH was found to be just above 5, but below 6, at which point the copper ions precipitate as Cu(OH)$_2$ [69]. **Cd-MOF-74** was shown to not only adsorb copper(II) ions from water but also detect them via photoluminescence quenching, with an impressive uptake of 190 mg g^{-1} of Cu(II) ions. The framework was highly selective toward Cu(II) ions in the presence of other metals in solution (such as Co(II) or Ni(II); using different solvents: H$_2$O, MeOH and DMF) [70]. In 2015, Zheng et al. investigated the selective adsorption properties of several zirconium-based MOFs for copper(II) over nickel(II) ions. **UiO-66(Zr)-2COOH** was found to be an excellent Cu(II) adsorbent, which was attributed to chelation by the two carboxyl groups. The functionalization of UiO-66(Zr) with carboxyl groups was found to significantly increase copper adsorption compared to the bare MOF. In addition, the MOF modified with only one carboxyl group adsorbs minimal copper. The capacity for Cu(II) adsorption increased with increasing pH from 4 to 6, at which point it reached its maximum [71]. Copper(II) adsorption on **ZIF-8** was examined in 2015 by Zheng et al. The MOF was reported to have excellent preferential Cu(II) adsorption properties over other metal ions. The adsorption process was found to be fairly fast, reaching equilibrium at 20 min and the maximum adsorption capacity was reported to be 224 mg g^{-1} [72]. Finally, another study on copper(II) adsorption *via* a transmetallation mechanism in **ZIF-8** was reported on by Zhang et al. in 2016. The unmodified MOF was synthesized at room temperature and its adsorption capacity was found to be stable between pH 3 and 6. The loss of effectiveness at pH lower than 3 was suggested to be due to the donor nitrogen of the MOF being protonated which causes reduction in its ability to coordinate the copper(II) ions. The optimal pH was found to be 5 where the framework exhibited an unprecedented adsorption capacity of 800 mg g^{-1}. Fig. 16 shows a proposed adsorption mechanism for Cu(II) ions in ZIF-8. It should be noted that when using transmetallation as an adsorption mechanism for metal ions, the toxicity of the metal ions (in this case zinc) that are replaced (i.e., those which end up in the water being treated) should be considered [73]. Separation of radioactive metals (such as ^{137}Cs, ^{90}Sr, ^{238}U, ^{79}Se, ^{99}Tc) using MOFs is an emerging area of research and has been discussed elsewhere [74–76].

3. Conclusions

There is much urgency when it comes to the control of heavy metal pollution within our environment. And while some of the pollution stems from natural sources, such as precipitation from rocks into ground and surface waters, much of the heavy metal contamination originates from anthropogenic activities related to industry, urbanization, or farming. Surface and groundwater are the main means of transportation for such pollutants, and as a crucially important resource for human populations, effective removal of contaminants from such sources is of utmost importance. Among many methods available, removal of heavy metals from water using metal–organic frameworks has become an increasingly popular research topic across the world. This review has summarized a number of contemporary research articles across a diverse range of disciplines addressing the issue of heavy metal removal from water using MOFs, and has aimed to look at data available and present it in an accessible and clear manner. The information has been sorted according to the heavy metals targeted, the MOFs used and their effectiveness, and working conditions. The intended purpose of this review is to produce a landscape view of this research area, as well as to provide an easily accessible summary of data available.

It is apparent that this steadily growing research area has quite a variety of adsorbents already available, with many reported MOFs having desirable features for adsorptive removal of heavy metals–many of which can be post-synthetically modified to further target specific contaminants, have wide-ranging adsorption mechanisms and capacities ranging anywhere from hundreds to a few mg g^{-1}, requiring anywhere between 10 min and a week of contact with the solution. In addition, the MOF adsorbents can function within either a wide range of pH values, or only within a (sometimes very) narrow window, be it of acidic, neutral or basic pH. Besides their high potential in selective adsorption and separation of heavy metal ions from water it is worth noting that a major challenge faced by majority of the MOFs is their poor water stability. Detailed information about the water and chemical stability of MOFs has already been thoroughly reviewed elsewhere [77,78].

What this overview shows, is that there is not clearly one single "best" MOF property that makes the material an effective adsorbent. Overall, there are still opportunities for more detailed studies, in particular toward understanding the adsorption mechanism of heavy metals in different MOFs. Engineered forms of MOFs should also be tested and methods of employing MOFs and MOF composites as adsorbents should be considered such as their use in filters which are either permanent (for frameworks which can be reused) or one-time use (where the MOF filters are perishable and need to be exchanged). Finally, more standardized testing of MOF materials against various water contaminants in addition to a better understanding of desirable properties for MOF-based adsorbents will help to propel this application forward in the future for this promising class of porous materials.

Appendix A. Supplementary data

Supplementary data associated with this article can be found, in the online version, at https://doi.org/10.1016/j.ccr.2017.12.010.

References

[1] M.A. Barakat, Arab. J. Chem. 4 (2011) 361–377.
[2] F.R. Siegel, Environmental Geochemistry of Potentially Toxic Metals, Springer, Berlin Heidelberg, Berlin, 2002.
[3] H.B. Bradl, Heavy Metals in the Environment: Origin, Interaction and Remediation, 1st ed., Elsevier Academic Press, London, 2005.
[4] B. Alloway, Heavy Metals in Soils, Blackie Academic and Professional, London, 1995.

[5] J.I. Drever, The Geochemistry of Natural Waters: Surface and Groundwater Environments, Prentice Hall, Upper Saddle River, NJ, 1997.
[6] F.R. Siegel, J. Geochem. Explor. 38 (1990) 265–283.
[7] D.C. Adriano, Trace Elements in Terrestrial Environments, Springer SBM, New York, 2001.
[8] F. Fu, Q. Wang, J. Environ. Manage. 92 (2011) 407–418.
[9] T. Pradeep, T. Anshup, Thin Solid Films 517 (2009) 6441–6478.
[10] A.R. Mahdavian, M.A.-S. Mirrahimi, Chem. Eng. J. 159 (2010) 264–271.
[11] E. Erdem, N. Karapinar, R. Donat, J. Colloid Interface Sci. 280 (2004) 309–314.
[12] Y. Zhao, Environ. Eng. Sci. 37 (2016) 443–454.
[13] R.J. Kuppler, D.J. Timmons, Q.R. Fang, J.R. Li, T.A. Makal, M.D. Young, D.Q. Yuan, D. Zhao, W.J. Zhuang, H.C. Zhou, Coord. Chem. Rev. 253 (2009) 3042–3066.
[14] O.M. Yaghi, M. O'Keeffe, N.W. Ockwig, H.K. Chae, M. Eddaoudi, J. Kim, Nature 423 (2003) 705–714.
[15] H. Furukawa, N. Ko, Y.B. Go, N. Aratani, S.B. Choi, E. Choi, A.Ö. Yazaydin, R.Q. Snurr, M. O'Keeffe, J. Kim, O.M. Yaghi, Science 329 (2010) 424–428.
[16] P. Li, N.A. Vermeulen, C.D. Malliakas, D.A. Gómez-Gualdrón, A.J. Howarth, B.L. Mehdi, A. Dohnalkova, N.D. Browning, M. O'Keeffe, O.K. Farha, Science 356 (2017) 624–627.
[17] Y.K. Park, S.B. Choi, H. Kim, K. Kim, B.-H. Won, K. Choi, J.-S. Choi, W.-S. Ahn, N. Won, S. Kim, D.H. Jung, S.-H. Choi, G.-H. Kim, S.-S. Cha, Y.H. Jhon, J.K. Yang, J. Kim, Angew. Chem. Int. Ed. 46 (2007) 8230–8233.
[18] I. Senkovska, S. Kaskel, Chem. Commun. 50 (2014) 7089–7098.
[19] J. An, O.K. Farha, J.T. Hupp, E. Pohl, J.I. Yeh, N.L. Rosi, Nat. Commun. 3 (2012) 604.
[20] O.K. Farha, I. Eryazici, N.C. Jeong, B.G. Hauser, C.E. Wilmer, A.A. Sarjeant, R.Q. Snurr, S.T. Nguyen, A.Ö. Yazaydin, J.T. Hupp, J. Am. Chem. Soc. 134 (2012) 15016–15021.
[21] A.J. Howarth, Y. Liu, J.T. Hupp, O.K. Farha, CrystEngComm 17 (2015) 7245–7253.
[22] S. Li, Y. Chen, X. Pei, S. Zhang, X. Feng, J. Zhou, B. Wang, Chin. J. Chem. 34 (2016) 175–185.
[23] Z. Hasan, S.H. Jhung, J. Hazard. Mater. 283 (2015) 329–339.
[24] B.-J. Zhu, X.-Y. Yu, Y. Jia, F.-M. Peng, B. Sun, M.-Y. Zhang, T. Luo, J.-H. Liu, X.-J. Huang, J. Phys. Chem. C 116 (2012) 8601–8607.
[25] M.P. Jian, B. Liu, G.S. Zhang, R.P. Liu, X.W. Zhang, Colloids Surf., A: Physicochem. Eng. Asp. 465 (2014) 67–76.
[26] B. Liu, M.P. Jian, R.P. Liu, J.F. Yao, X.W. Zhang, Colloids Surf., A: Physicochem. Eng. Asp. 481 (2015) 358–366.
[27] T.A. Vu, G.H. Le, C.D. Dao, L.Q. Dang, K.T. Nguyen, Q.K. Nguyen, P.T. Dang, H.T.K. Tran, Q.T. Duong, T.V. Nguyen, G.D. Lee, RSC Adv. 5 (2015) 5261–5268.
[28] J. Li, Y.N. Wu, Z.H. Li, M. Zhu, F.T. Li, Water Sci. Technol. 70 (2014) 1391–1397.
[29] Z.Q. Li, J.C. Yang, K.W. Sui, N. Yin, Mater. Lett. 160 (2015) 412–414.
[30] C.H. Wang, X.L. Liu, J.P. Chen, K. Li, Sci. Rep. 5 (2015) 10.
[31] C.O. Audu, H.G.T. Nguyen, C.-Y. Chang, M.J. Katz, L. Mao, O.K. Farha, J.T. Hupp, S. T. Nguyen, Chem. Sci. 7 (2016) 6492–6498.
[32] Y. Wang, G.Q. Ye, H.H. Chen, X.Y. Hu, Z. Niu, S.Q. Ma, J. Mater. Chem. A 3 (2015) 15292–15298.
[33] A. Chakraborty, S. Bhattacharyya, A. Hazra, A.C. Ghosh, T.K. Maji, Chem. Commun. 52 (2016) 2831–2834.
[34] Q.-R. Fang, D.-Q. Yuan, J. Sculley, J.-R. Li, Z.-B. Han, H.-C. Zhou, Inorg. Chem. 49 (2010) 11637–11642.
[35] H. Saleem, U. Rafique, R.P. Davies, Microporous Mesoporous Mater. 221 (2016) 238–244.
[36] A. Abbasi, T. Moradpour, K. Van Hecke, Inorg. Chim. Acta 430 (2015) 261–267.
[37] J.M. Zhang, Z.H. Xiong, C. Li, C.S. Wu, J. Mol. Liquids 221 (2016) 43–50.
[38] E. Tahmasebi, M.Y. Masoomi, Y. Yamini, A. Morsali, Inorg. Chem. 54 (2014) 425–433.
[39] E. Rahimi, N. Mohaghegh, Mine Water Environ. 35 (2015) 18–28.
[40] F. Zou, R.H. Yu, R.G. Li, W. Li, ChemPhysChem 14 (2013) 2825–2832.
[41] Q.X. Yang, Q.Q. Zhao, S.S. Ren, Q.Q. Lu, X.M. Guo, Z.J. Chen, J. Solid. State Chem. 244 (2016) 25–30.
[42] K. Wang, X.R. Tao, J.Z. Xu, N. Yin, Chem. Lett. 45 (2016) 1365–1368.
[43] A. Maleki, B. Hayati, M. Naghizadeh, S.W. Joo, J. Ind. Eng. Chem. 28 (2015) 211–216.
[44] L.-L. Li, X.-Q. Feng, R.-P. Han, S.-Q. Zang, G. Yang, J. Hazard. Mater. 321 (2017) 622–628.
[45] Q. Zhang, J.C. Yu, J.F. Cai, L. Zhang, Y.J. Cui, Y. Yang, B.L. Chen, G.D. Qian, Chem. Commun. 51 (2015) 14732–14734.
[46] X.Y. Li, X.Y. Gao, L.H. Ai, J. Jiang, Chem. Eng. J. 274 (2015) 238–246.
[47] L. Aboutorabi, A. Morsali, E. Tahmasebi, O. Buyukgungor, Inorg. Chem. 55 (2016) 5507–5513.
[48] S. Rapti, A. Pournara, D. Sarma, I.T. Papadas, G.S. Armatas, Y.S. Hassan, M.H. Alkordi, M.G. Kanatzidis, M.J. Manos, Inorg. Chem. Front. 3 (2016) 635–644.
[49] C.-C. Wang, X.-D. Du, J. Li, X.-X. Guo, P. Wang, J. Zhang, Appl. Catal., B: Environ. 193 (2016) 198–216.
[50] R. Ricco, K. Konstas, M.J. Styles, J.J. Richardson, R. Babarao, K. Suzuki, P. Scopece, P. Falcaro, J. Mater. Chem. A 3 (2015) 19822–19831.
[51] A. Jamali, A.A. Tehrani, F. Shemirani, A. Morsali, Dalton Trans. 45 (2016) 9193–9200.
[52] Q.D. Qin, Q.Q. Wang, D.F. Fu, J. Ma, Chem. Eng. J. 172 (2011) 68–74.
[53] J.M. Rivera, S. Rincon, C. Ben Youssef, A. Zepeda, J. Nanomater. (2016) 9.
[54] F. Ke, L.G. Qiu, Y.P. Yuan, F.M. Peng, X. Jiang, A.J. Xie, Y.H. Shen, J.F. Zhu, J. Hazard. Mater. 196 (2011) 36–43.
[55] L.F. Liang, Q.H. Chen, F.L. Jiang, D.Q. Yuan, J.J. Qian, G.X. Lv, H. Xue, L.Y. Liu, H.L. Jiang, M.C. Hong, J. Mater. Chem. A 4 (2016) 15370–15374.
[56] L.J. Huang, M. He, B.B. Chen, B. Hu, J. Mater. Chem. A 3 (2015) 11587–11595.
[57] F. Luo, J.L. Chen, L.L. Dang, W.N. Zhou, H.L. Lin, J.Q. Li, S.J. Liu, M.B. Luo, J. Mater. Chem. A 3 (2015) 9616–9620.
[58] S. Halder, J. Mondal, J. Ortega-Castro, A. Frontera, P. Roy, Dalton Trans. 46 (2017) 1943–1950.
[59] T. Liu, J.X. Che, Y.Z. Hu, X.W. Dong, X.Y. Liu, C.M. Che, Chem. Eur. J. 20 (2014) 14090–14095.
[60] K.K. Yee, N. Reimer, J. Liu, S.Y. Cheng, S.M. Yiu, J. Weber, N. Stock, Z.T. Xu, J. Am. Chem. Soc. 135 (2013) 7795–7798.
[61] N.D. Rudd, H. Wang, E.M.A. Fuentes-Fernandez, S.J. Teat, F. Chen, G. Hall, Y.J. Chabal, J. Li, ACS Appl. Mater. Interfaces 8 (2016) 30294–30303.
[62] S. Bhattacharjee, Y.R. Lee, W.S. Ahn, CrystEngComm 17 (2015) 2575–2582.
[63] M.R. Sohrabi, Microchim. Acta 181 (2013) 435–444.
[64] X.B. Luo, T.T. Shen, L. Ding, W.P. Zhong, J.F. Luo, S.L. Luo, J. Hazard. Mater. 306 (2016) 313–322.
[65] M. Mon, F. Lloret, J. Ferrando-Soria, C. Marti-Gastaldo, D. Armentano, E. Pardo, Angew. Chem. Int. Ed. 55 (2016) 11167–11172.
[66] Y.Y. Xiong, J.Q. Li, L.L. Gong, X.F. Feng, L.N. Meng, L. Zhang, P.P. Meng, M.B. Luo, F. Luo, J. Solid State Chem. 246 (2017) 16–22.
[67] X.Q. Cheng, M. Liu, A.F. Zhang, S. Hu, C.S. Song, G.L. Zhang, X.W. Guo, Nanoscale 7 (2015) 9738–9745.
[68] J.E. Conde-Gonzalez, E.M. Pena-Mendez, S. Rybakova, J. Pasan, C. Ruiz-Perez, J. Havel, Chemosphere 150 (2016) 659–666.
[69] N. Bakhtiari, S. Azizian, J. Mol. Liquids 206 (2015) 114–118.
[70] T.T. Zheng, J. Zhao, Z.W. Fang, M.T. Li, C.Y. Sun, X. Li, X.L. Wang, Z.M. Su, Dalton Trans. 46 (2017) 2456–2461.
[71] Y.T. Zhang, X.D. Zhao, H.L. Huang, Z.J. Li, D.H. Liu, C.L. Zhong, RSC Adv. 5 (2015) 72107–72112.
[72] Y.J. Zhao, Y.C. Pan, W. Liu, L.X. Zhang, Chem. Lett. 44 (2015) 758–760.
[73] Y. Zhang, Z. Xie, Z. Wang, X. Feng, Y. Wang, A. Wu, Dalton Trans. 45 (2016) 12653–12660.
[74] C. Xiao, M.A. Silver, S. Wang, Dalton Trans. (2017).
[75] B. Aguila, D. Banerjee, Z. Nie, Y. Shin, S. Ma, P.K. Thallapally, Chem. Commun. 52 (2016) 5940–5942.
[76] S. Sarina, A. Bo, D. Liu, H. Liu, D. Yang, C. Zhou, N. Maes, S. Komarneni, H. Zhu, Chem. Mater. 26 (2014) 4788–4795.
[77] N.C. Burtch, H. Jasuja, K.S. Walton, Chem. Rev. 114 (2014) 10575–10612.
[78] A.J. Howarth, Y. Liu, P. Li, Z. Li, T.C. Wang, J.T. Hupp, O.K. Farha, Nat. Rev. Mater. 1 (2016) 15018.